Università degli Studi di Ferrara

DOTTORATO DI RICERCA IN
MEDICINA MOLECOLARE E FARMACOLOGIA

CICLO XXXII

COORDINATORE Prof. Di Virgilio Francesco

The P2X7 receptor modulates extracellular ATP levels cell to cell communication and chemoresistance in oncogenesis

Settore Scientifico Disciplinare MED/04

Dottoranda
Dott. Pegoraro Anna

Tutore
Prof. Adinolfi Elena

Anni 2016/2019

TABLE OF CONTENTS

RESULTS

CHAPTER I

Role of extracellular ATP in acute myeloid leukemia and P2X7 receptor in chemotherapyresistance

ABBREVIATIONS

A740003	N-[1-[[(Cyanoamino)(5-quinolinylamino)methylene]-2,2-dimethylpropyl]-3,4-dimethoxybenzeneacetamide
ADP	adenosine diphosphate
AIRTUM	associazione italiana registro tumouri
AML	acute myeloid leukemia
AMP	adenosine monophsophate
AKT	seronine/threonine kinase
ARA-C	cytosine arabinoside
ATP	adenosine triphosphate
AZ10606120	N-[2-[[2-[(2-hydroxyethyl)amino]-5-quinolinyl]-2-tricyclo[3.3.1.13,7]dec-1-ylacetamide dihydrochloride
BzATP	2'-3'- (4'- benzoil)- benzoil-ATP
COX	cyclooxygenase
DAMP	damage associated molecular pattern
DNR	daunorubicin
eATP	extracellular ATP
EV	extracellular vesicle
HEK	human embryonic kidney
HIF	hypoxia-inducible factor
ICD	immunogenic cell death
IFN-γ	interferon gamma
IL	interleukin
MDS	myelodisplastic sindrome
miRNA	microRNA
MV	microvesicle
NFATc1	nuclear factor activated T-cells
NF-kB	nuclear factor kappa-light chain-enhancer of activated B cells
NLRP3	NOD-like receptor pyrin-domain-containing 3
PI3K	phosphoinositide 3-kinases
pmeLUC	membrane luciferase
TGF-β	transforming growth factor beta
TME	tumour microenvironment

TNF-α	tumour necrosis factor alfa
VEGF	vascular endothelial growth factor

INTRODUCTION

CHAPTER 1: ADENOSINE TRIPHOSPHATE

1.1 Adenosine triphosphate as extracellular messenger

Adenosine triphosphate (ATP) is a nucleotide originally isolated by Karl Lohmann in 1929 and it is the main intracellular energy molecule that chemically consists of three components: an adenine, the sugar ribose and the triphosphate. In several metabolic reactions the adenine and sugar group remain unchanged while the triphosphate is converted in di- and monophosphate giving rise to ADP and AMP respectively. Every time that a phosphate group is cleaved from ATP, a high energy transfer occurs to drive many processes as different as muscle contraction, nerve impulse propagation, active ion transport and macromolecules synthesis. ATP can be produced through three main cellular processes: glycolysis, tricarboxylic acid cycle and oxidative phosphorylation. The concentration of ATP within cells is very high in the millimolar range. On the contrary, the extracellular ATP (eATP) levels are very low, in the nanomolar range [1]. In 1970, Burnstock and colleagues have shown the release of ATP from non-adrenergic inhibitory nerves [2] and in 1972 they formulated the "purinergic signalling hypothesis" in which ATP was described as an extracellular messenger [3]. Recently, evidence demonstrates the accumulation of high levels of ATP at inflammatory sites and in the tumour microenvironment (TME) [4]. ATP can be secreted in the extracellular space from stressed or dying cells, in response to mechanical stress, plasma membrane damage, tumour necrosis, hypoxia [5, 6] and in response to chemotherapeutic drugs [7] or it can be spontaneously released from both immune and cancer cells through membrane channels and non-selective membrane pores such as connexins and pannexin 1 [8, 9]. Once in the extracellular space, ATP can be converted to ADP and AMP by the ectonucleotidases CD39, which can then converted in adenosine by ectonucleotidases CD73. CD39 and CD73 are the main enzymes responsible for ATP degradation in the extracellular environment [10].

1.2 ATP release during immunogenic cell death

In the field of anticancer therapy, the use of cytotoxic antineoplastic agents has obtained great success by directly killing cancer cells or inducing their senescence. However, growing evidence demonstrates that some of these antitumour agents stimulate a specific

immune anticancer response, that determines a favourable long-term outcome. Chemotherapeutics, such as anthracyclines and oxaliplatin, and radiotherapy are able to induce a particular type of cell death named immunogenic cell death (ICD) characterized by the activation of an antitumour immune response against dead-cell antigens [11]. During ICD, dying cells release damage-associated molecular patterns (DAMPs), that act as danger signals for the recruitment and activation of neutrophils, macrophages and dendritic cells [12]. ATP has a central role in ICD, it is released as DAMP and in the extracellular space behaves like a pro-inflammatory stimulus activating P2X7 receptor (P2X7) expressed on dendritic cells and macrophages stimulating NOD-like receptor pyrin-domain-containing 3 (NLRP3) inflammasome that in turn drives IL-1β proteolytic maturation and release [13]. IL-1β induces tumour antigens presentation by dendritic cells to $CD4^+$ and $CD8^+$ T lymphocytes [14]. ATP secretion can occur via plasma membrane channels such as pannexin1, transporters of the ATP-binding cassette family, the cystic fibrosis transmembrane conductance regulator and P2X7 itself [15]. Then in the tumour microenvironment, the immunosuppressive ectonucleotidases CD39 and CD73 have a central role in the regulation of ATP levels, thus they contribute to the anticancer immune response elicited during ICD [16]. In fact, the overexpression of CD39 and CD73 by tumour cells impairs the efficacy of chemotherapy [17].

1.3 Measurement of extracellular ATP

It is possible to measure eATP thanks to different probes derived from luciferase, an enzyme present in firefly *Photinus pyralis*, that is able to catalyse the oxygenation of the substrate luciferin using ATP and molecular oxygen finally causing photons emission. The standard assay used to measure ATP concentration consists of the use of soluble luciferase/luciferin molecules that are added in the cell culture medium to measure the concentration of ATP diffused in the supernatant after cell stimulation. The first probe specifically designed to measure eATP was obtained by Dubyak and colleagues and named A-luciferase. A-luciferase consists of an IgG-binding domain that allows the attachment of this chimeric protein to the extracellular membrane for the detection of surface-localized ATP [18]. Instead, Pellegatti and colleagues have introduced a novel genetically encoded probe named pmeLUC (Figure 1), in which the presence of the folate receptor leader sequence, in frame with luciferase construct, targets the luciferase protein to the external layer of the plasma membrane to detect ATP in the extracellular space close to the cell

surface [19]. Interestingly, this probe is sensitive only to ATP and its affinity to this nucleotide is very low around 5-10 µM. pmeLUC can be transfected directly into the cancer cells used to obtain *in vivo* tumour or into reporter cells. *In vivo* ATP concentration measured with pmeLUC is in the range of 100-500 micromoles per litre, which is higher than that found in the healthy tissue [4, 20].

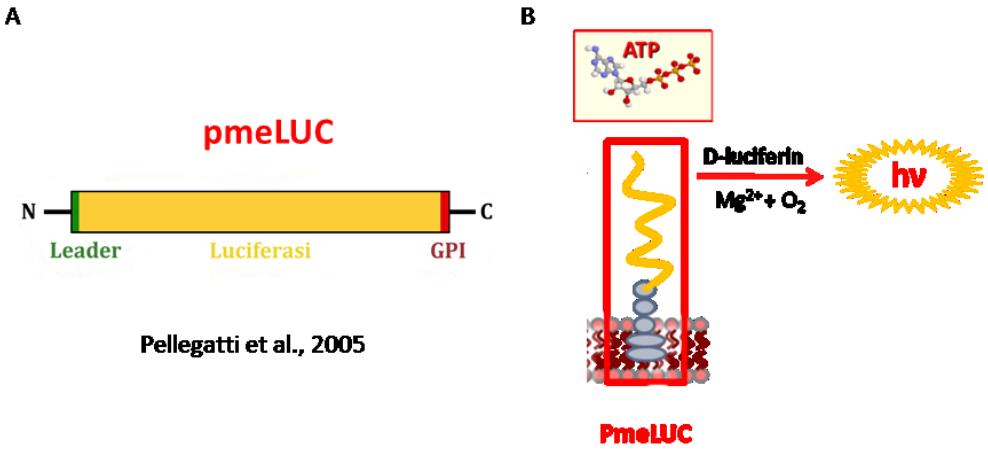

Figure 1 Structure of the pmeLUC construct

(**A**) pmeLUC structure comprising the full-lenght coding sequence of luciferase inserted in-frame between the N-terminal, leader sequence (26 aa) and the C-terminal GPI anchor (28 aa) of the folate receptor.(**B**) Chemical reaction catalysed by luciferase.

CHAPTER 2: P2 PURINERGIC RECEPTORS

2.1 P2 RECEPTOR SUBFAMILIES

In the early 1990s, ATP receptors were described in immune and cancer cells, suggesting the importance of ATP as extracellular messenger not only in the neuroscience field but also in immunology and oncology [21-23]. P2 purinergic receptors (P2Rs) are plasma membrane receptors activated by extracellular purine or pyrimidine nucleotides. P2Rs are expressed in many different cell types and are involved in several physiological and pathophysiological responses. On the basis of pharmacological properties and functional features, P2Rs are classified into two different subfamilies: metabotropic P2Y and ionotropic P2X receptors [24]. P2YRs are seven transmembrane domains, G-protein coupled receptors and their activation is linked to a signal cascade that regulates Ca^{2+} ions flow by the interactions with G proteins [22]. According to their coupling to specific G protein, P2YRs can be further subdivided into different subfamilies: P2Y1R, P2Y2R, P2Y4R and P2Y6R (activate phospholipase Cβ via G_q), and P2Y12R, P2Y13R and P2Y14R (inhibit adenylyl cyclase via G_i). Instead, P2Y11R couples both G_q and G_s activating intracellular Ca^{2+} rise and the increase of cAMP levels. ATP interacts only with P2Y11, while for other P2YRs, pyrimidine nucleotides or ADP are the preferred and more potent agonists [25]. P2XRs are ATP gated ion channels permeable to Na^+, K^+ and Ca^{2+} and belong to the combination of seven different subunits (P2X1-7) [26]. Each subunit consists of two transmembrane domains, an extracellular loop, intracellular carboxy and amino-terminal tails [27]. The subunits can assemble in homotrimeric or heterotrimeric channels with different functional and pharmacological properties. P2X1, 2, 3, 4 and 6 subunits can form homotrimeric as well as heterotrimeric channels, instead P2X5 subunit is functional only in association with P2X1, 2 and 4 [28]. P2X7 subunit forms only homotrimeric channels, even if they can assemble under particular conditions as homoexamers [26, 29]. P2X1R, P2X2R, P2X3R and P2X4R show a very low affinity for ATP (micromolar range), while P2X7 is activated by higher ATP concentrations (0,5-1 mM) [26]. Nevertheless, all P2XRs induce the flux of Ca^{2+}, Na^+ or K^+ causing changes in intracellular ions concentration, the main mechanism associated with P2XRs to trigger signal transduction pathway. P2YRs and P2XRs are expressed in almost all cell types including cancer and immune cells [30, 31]. They are involved in several processes such as cell proliferation, differentiation and death [32] as well as immune responses, inflammation, pain, platelet aggregation and endothelial-mediated vasodilatation [33].

2.2 P2X7 receptor structure

The human P2X7 receptor gene is located on chromosome 12q24.31 and close to the P2X4R gene [34]. The P2X7 subunit, with its 595 amino acids, is the longest protein among P2X family [35] and it assembles to form a trimeric receptor. It consists in a short intracellular N-terminal tail (26 aa), a large extracellular loop (282 aa) that participates in the formation of ATP binding site, two transmembrane helices (24 aa each) and a long cytoplasmic carboxy-terminal tail (239 aa) [35]. The crystal structures of giant panda and rat P2X7 were recently described [36, 37] and they are similar to the structure of the zebrafish P2X4R [27], that has been previously used to describe the theoretical three-dimensional structure of P2X7. The three-dimensional monomer structure has a dolphin-like shape [38], where the large extracellular loop constitutes the main body (head, flippers and dorsal fin) and the two transmembrane helices form the dolphin tail (Figure 2).

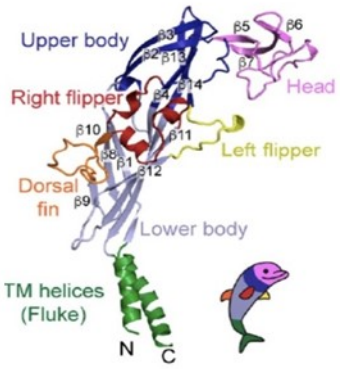

Figure 2 Three-dimensional structure of P2X7 subunit

The shape of P2X7 subunit is compared to a dolphin with the subdivision of the monomer regions in head, flippers and dorsal fin constituted by the large extracellular loop, and the dolphin tail constituted by the two transmembrane tail [31].

The crystal analysis of homotrimeric P2X7 revealed that the three distinct subunits interact in the area corresponding to the dolphin's upper body and also the opening of the channel requires the binding of three ATP molecules [38]. Each of these ATP molecules binds a site derived from the interaction between two neighbouring monomers and induces conformational rearrangements in P2X7 structure to allow channel opening. Moreover, the analysis of the crystal structure of panda P2X7 showed the presence of an allosteric binding site different from ATP pocket and localized between two adjacent monomers. Full-length structure of rat P2X7 has been recently described showing the importance of

palmitoylation preventing desensitization and opening the way for further developments of P2X7 blocking drugs and protein-protein interactions [37].

An interesting property of P2X7 is its dual function. P2X7 behaves like a cation-selective channel (Na^+, Ca^{2+}, K^+) upon ATP binding, moreover stimulated with millimolar ATP concentrations it causes the opening of a large non-selective pore permeable to small aqueous solutes (up to 900 Da) such as ethidium bromide, YO-Pro or Lucifer yellow [35] (Figure 3). The pore formation is reversible, removal of ATP in a few minutes from its addition induces the reconstitution of cell membrane integrity [39], and its opening is due to the presence of the long carboxy-terminal tail [35, 40]. Pore formation is associated with cytotoxic activity in presence of high ATP levels, instead tonic activation of P2X7 with low autocrine or paracrine stimulation with ATP supports a trophic effect [41].

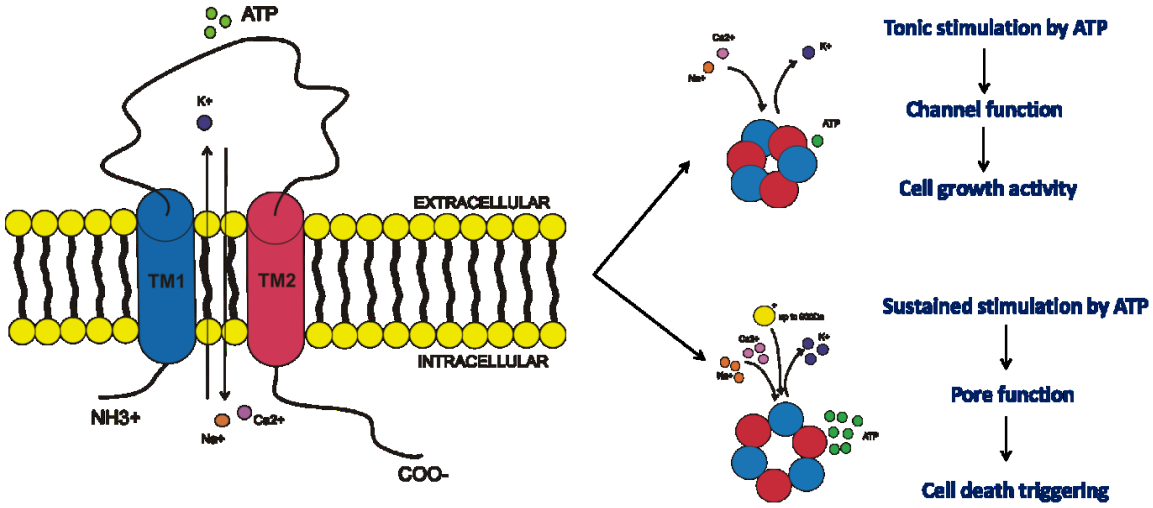

Figure 3 Dual function of P2X7 receptor.

Representative structure of P2X7 receptor and its functions.

2.3 P2X7 splice variants

The human P2X7 gene consists of 13 exons and ten different P2X7 splice variants were identified in humans (P2X7A-J) [42]. P2X7A is the first variant identified and corresponds to the full-length protein, P2X7B, P2X7ER, P2X7GR [42] lack the extended C-terminal tail, P2X7GR and P2X7HR have an inserted additional exon, while P2X7CR, P2X7DR, P2X7ER and P2X7FR lacks respectively exon 4, exon 5, exons 7 and 8, exons 4 and 8 [42]. Additional variants including P2X7IR derived from a point mutation in the first intron of P2X7 that generates a null allele [43] and P2X7JR that is truncated after exon 7

and it is non- functional [44]. Among these splice variants, the only functional is P2X7B that is widely expressed in many human tissues. It retains an intron between exons 10 and 11, causing the addition of 18 extra amino acids after residue 346 followed by a stop codon [42]. P2X7B is unable to form the large pore and maintains only the channel function [40]. In recent years, it was shown that P2X7B isoform exerts a growth-promoting activity and its co-expression with P2X7A potentiates cell proliferation inducing an increase of Ca^{2+} flux and NFATc1 activity [40, 45-47]. Nevertheless, P2X7A and P2X7B share the same pharmacological response to agonists and antagonists [42].

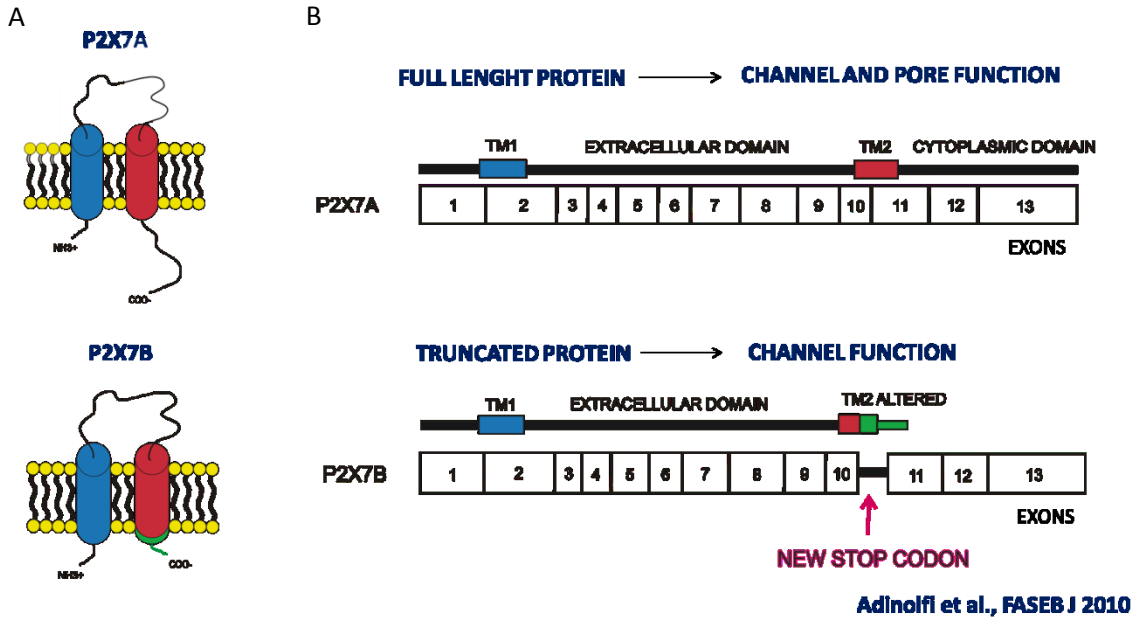

Figure 4 Structure of P2X7 receptor isoforms A and B. (**A**) Representation of P2X7A and P2X7B expressed on cell membrane. (**B**) Representation of the full length protein P2X7A and truncated P2X7B.

2.4 P2X7 receptor agonists and antagonists

ATP is the natural ligand of P2X7 receptor. Unlike other members of P2XR family, P2X7 is activated by high concentrations of ATP (millimolar range). A synthetic ATP derived compound, 2'(3')-O-(4-benzoylbenzoyl) adenosine-5'-triphosphate (Bz-ATP) is a better agonist at P2X7 with a potency that is 5-10 fold greater than ATP [48]. However, BzATP is not a selective agonist at P2X7 as it can activate also P2X1R and P2X3R [49]. The P2X7 is considered an interesting therapeutic target due to its involvement in inflammatory disorders, pain and cancer. Therefore, several P2X7 antagonists were identified. Classical nonselective P2X7 antagonists are suramin and pyridoxal phosphate-6-azopheny-2',4' disulfonate (PPADS) that block the receptor with low affinity and show non-competitive

antagonism [48]. Brilliant blue G (BBG) is a more potent and selective antagonist, while KN62 potently blocks P2X7 function in a non-competitive fashion. Oxidized-ATP (oATP) is an irreversible inhibitor and blocks also P2XR1 and P2X2R [50]. Over the years, the use of these molecules was replaced by more effective and selective antagonists including A438079, A740003 and AZ10606120. A438079 is a reversible and competitive blocker and shows little activity at other cell membrane receptors and ion channels [51]. A740003 is a highly specific and potent antagonist with an IC50 of 40 nM for human P2X7. Similar to A438079, A740003 mediates changes in intracellular calcium concentrations in a competitive fashion. In addition, it is more potent than A438079 to inhibit the effect of BzATP on IL-1β release and pore formation in differentiated human THP-1 cells [52]. Interestingly, A740003 has sufficient bioavailability following intraperitoneal administration thus allowing for its use *in vivo* experiments [51, 52]. In particular, A740003 demonstrated to attenuate nociception in animal models of persistent neuropathic and inflammatory pain [52, 53] and reduce neuroblastoma and melanoma tumour growth in mice [54, 55]. Another P2X7 antagonist is AZ10606120, binds to a site different but correlated to ATP binding pocket and acts as a negative allosteric modulator. Also this P2X7 antagonist inhibits tumour growth [54, 55] and shows anti-angiogenic effects in mice [55].

2.5 P2X7 receptor in inflammation

The P2X7 receptor has an important role in inflammation and immunity [56] and it is expressed by virtually all immune cell types among which macrophages, monocytes, dendritic cells, microglia, T and B lymphocytes, mast and natural killer cells [57]. The best-recognized function ascribed to P2X7 is the release of mature IL-1β and IL-18 cytokines [58]. IL-1β is a central player in the inflammatory cascade and it activates signal transduction pathways such as MAPK and NF-kB, inducing the over-expression of molecules involved in inflammation such as COX-2, IL-6, chemokines and cellular adhesion molecules [59]. IL-18 has an important role in inflammation and in the immune response to infection [58]. Both IL-1β and IL-18 are released in the extracellular milieu as active molecules following the cleavage by caspase-1of their precursors pro-IL-1β and pro-IL-18. The best-recognized stimulus for IL-1β and IL-18 maturation and release is ATP acting at P2X7 [60]. During inflammation, ATP is released from dying and injured cells and activates P2X7 inducing K^+ efflux, which is crucial for NOD-like receptor pyrin-domain-containing 3 (NLRP3) inflammasome assembly that is necessary for the

maturation and release of IL-1β and IL-18 [60]. Other intracellular inflammatory pathways are influenced by P2X7, for example activation of the nuclear factor NF-kB that controls the expression of several inflammatory genes like TNFα, COX-2 and IL-1β itself [61], or activation of cyclo-oxygenase (COX-1) and expression of COX-2 leading to fever and pain via ERK/MAPK kinases and phospholipase A2 [62]. Given the important role in inflammation, it is not surprising that P2X7 is associated with several chronic inflammatory disorders. In respiratory diseases, the exposition to high oxygen concentration induces the activation of P2X7, inflammasome assembly and release of IL-1β causing inflammation of lung tissue. It was demonstrated the association between P2X7 and rheumatoid diseases such as rheumatoid arthritis [63], systemic lupus erythematosus [64] and in immune-related glomerulonephritis [65]. Moreover, P2X7 is associated with neurological disorders such as multiple sclerosis, Alzheimer's disease and amyotrophic lateral sclerosis [49].

2.6 P2X7 receptor and cancer

Several studies demonstrated the expression of P2X7 in different solid tumours like breast [66], prostate [67], colon [54], renal [54] and cervical cancers [68], melanoma [69], neuroblastoma [70] and papillary thyroid carcinoma [71] as well as blood malignancies among which chronic lymphocytic leukemia (CLL) [72], acute myeloid leukemia (AML) [73] and myelodysplastic syndrome [74]. P2X7 activation with endogenous ATP was associated to cancer cell proliferation [54, 55] and migration [75, 76], tumour immune response [77-81] and pain sensation [82]. During oncogenesis, P2X7 plays an important role in different pathways such as oncogene expression [55, 83], tumour vascularization [54, 55], and matrix degradation [76]. In a study by Adinolfi et al., it was demonstrated that HEK293 cells, that normally do not express P2X7, once transfected with the receptor showed an increase of intracellular ATP, higher mitochondrial potential and greater amount of basal mitochondrial Ca^{2+} as compared with controls [41]. Moreover, in neuroblastoma it was demonstrated that P2X7 behaves like a positive modulator of PI3K/Akt/HIF1-α network promoting tumour growth and vasculogenesis [55]. P2X7 promotes cell migration and extracellular matrix invasion modulating the expression of E-cadherin and matrix metalloproteinases 3 and 13 via Akt [84]. While, transforming growth factor-beta (TGF-β), a TME component, activates P2X7 causing cytoskeleton modifications and cell migration [85], that also are correlated to intracellular calcium concentration and phosphoinositide 3-kinases (PI3K) activation [86]. P2X7 directly induces an increase in intracellular calcium

concentration that activates the nuclear factor of activated T cell 1 (NFATc1) causing cell proliferation [45, 87]. Other pathways associated with P2X7 are the hypoxia-activated factor HIF1-α and its target gene VEGF, that provide essential nutrients to cancer cells via the formation of new blood vessels. In fact, it was demonstrated that P2X7 induces vessel formation in different cancer models increasing HIF1-α activity and VEGF secretion [54, 55, 83, 88]. Recently, in a study carried out by Solini and colleagues it was shown that the up-regulation of P2X7 and VEGF2 receptor is associated with the worsening of prostate cancer, while the silencing of both receptors ameliorates the prognosis for this disease [89]. Moreover, the overexpression of P2X7 is associated to negative prognosis and tumour progression in different solid and non-solid tumours such as acute and chronic lymphatic leukemia [72, 90], papillary thyroid carcinoma [91] and neuroblastoma [55]. Interestingly, P2X7 silencing or pharmacological blockade on cancer cells inhibits tumour growth in experimental xenograft models of neuroblastoma and melanoma [54, 81]. Nevertheless, some studies have reported a protective role for P2X7 in some cancers. Morrone and colleagues demonstrated an association between P2X7 increase expression and positive response to radiotherapy in patients affected by glioblastoma [92]. This observation was confirmed using a murine model of glioblastoma in which the lack of P2X7 reduced the efficacy of radiotherapy [93]. It is well known that radiations, as well as some chemotherapeutics, cause ATP secretion from dying cancer cells that can stimulate P2X7 expression by immune cells inducing a specific anti-cancer immune response.

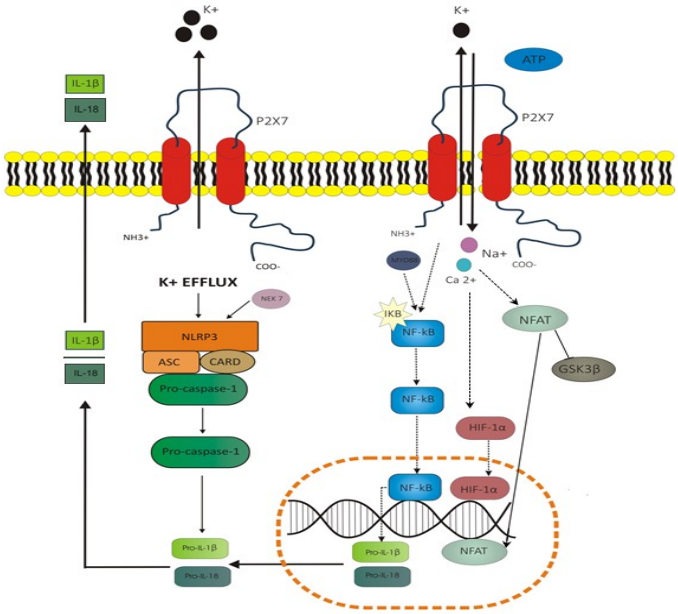

Figure 5 Schematic representation of pathways activated by P2X7 receptor during inflammation and cancer proliferation (from [60]).

CHAPTER 3: EXTRACELLULAR VESICLES

3.1 Characterization of extracellular vesicles

Increasing evidence suggests that intercellular communication is important for cells to grow and function normally. Recently, the release of extracellular vesicles (EVs) has been recognized as one of the main mechanisms used by cells to communicate. EVs are small lipid bilayer-delimited particles that are released from nearly all cell types, cancer cells included, by several biologic processes and in response to different stimuli [94]. They carry biologically active molecules including proteins, lipids, DNA, various RNA species such as mRNA, miRNA and lncRNA, metabolites and organelles. Thus, EVs have the capacity to transfer biomolecules from a parent cell into recipient cell, potentially influencing the recipient behaviour [95]. Different EV subtypes have been described based on size, molecular composition, function or method of separation [96]. Among them, the main three families are microvesicles, exosomes and apoptotic bodies. Microvesicles (MVs) are directly budded from the plasma membrane and their size ranges from 100 nm to 1000 nm. Like MVs, apoptotic bodies are formed by the outward budding of the plasma membrane and they range from 0.1 to 5 μm in diameter. They are released during cell apoptosis and they are characterized by immunogenic activity. Instead, exosomes, the smallest EV fraction with a size ranging from 30 to 150 nm, have an endosomal origin [94].

3.2 Extracellular vesicles in cancer

Tumour cells can constitutively release extracellular vesicles that act as messengers in communication between tumour cells and surrounding non-tumour cells in the neighbouring and distant microenvironment. In the contest of primary tumour, tumour-derived EV contributes to different biological events. For example, it was demonstrated that tumour-derived exosomes, containing TGF-β, drive the phenotype change of fibroblasts in myofibroblasts, favouring vascularization, tumour growth and local invasion [97], exosomes containing both mRNA and microRNA can be transferred to recipient cells and modulate gene expression [98] while tumour EV may induce in recipient cells epithelial to mesenchymal transition [99]. EVs released from primary tumour can move through blood circulation and influence the behaviour of many cell types at distant sites and mediate several biological processes such as angiogenesis, immune response and the formation of a pre-metastatic niche. EVs promote both immune suppression and activation,

suggesting the importance of cell type and EVs content in the modulation of the immune response. In some cases EVs can transfer tumour antigens to immune cells for antigen presentation to T cells to induce an immune response against the tumour [100]. Interestingly, tumour exosomes contain specific integrins that direct them to precise organs determining the so-called metastatic organotropism [101].

Extracellular ATP acts as a strong enhancer of membrane blebbing and vesicles shedding upon activation of its receptor P2X7. Evidence of the release of EVs from cancer cells following P2X7 stimulation is still missing. However, release of microvesicles (MVs) containing pro-inflammatory cytokines following P2X7 activation on immune cells is an established notion. Several studies demonstrated exocytosis of MVs carrying IL-1β from macrophages [102], microglia [103] and dendritic cells [104]. Other molecules such as IL-18 [105], TNF-α [106] and tissue factor [107] are released in EVs from macrophages and dendritic cells.

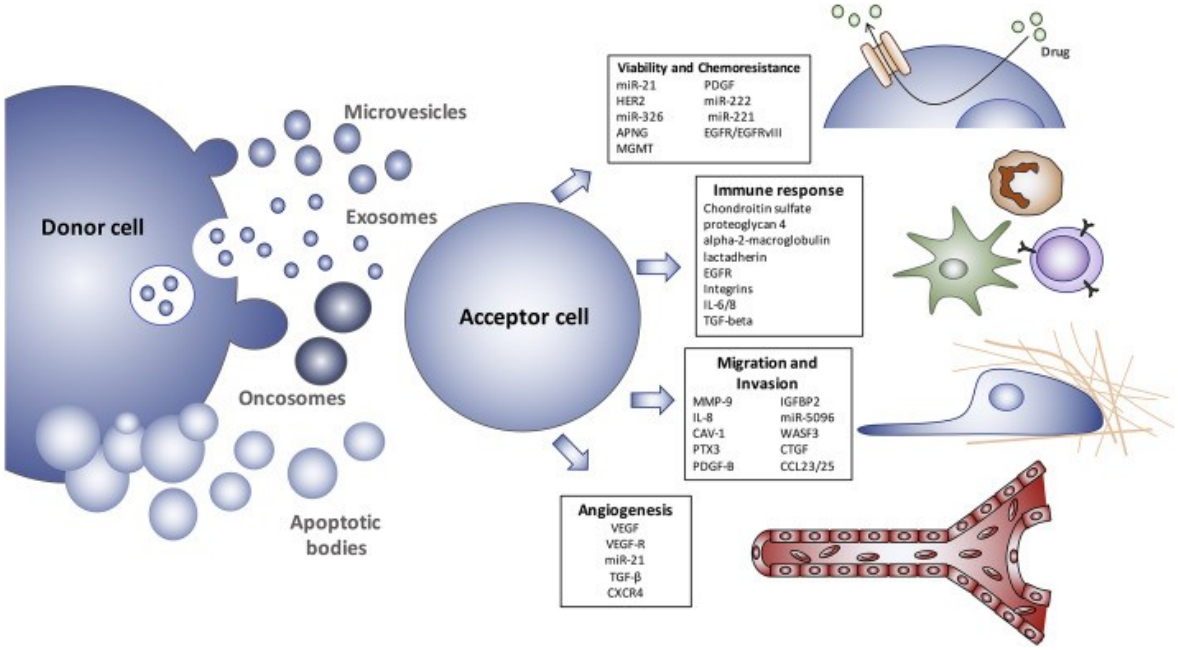

Figure 6 Schematic representation of extracellular vesicles release.

Cells can release different types of vesicles. The molecular contents of these vesicles vary depending on the cell of origin and can influence the behaviour of recipient cells. From [108].

3.3 miRNAs in extracellular vesicles

In recent years, several studies were focused on investigating the role of microRNAs (miRNAs) that are transferred among cells via extracellular vesicles. miRNAs are small, non-coding RNA molecules (21-23 nucleotides) that regulate transcriptional and post-

transcriptional gene expression [109]. miRNAs bind to complementary mRNA sequences resulting in gene silencing through translational suppression or target degradation [110]. The oncogenic profile of miRNA present in the extracellular vesicles depends on cancer type and may have different effects depending on the recipient cell type [111]. Actually, miRNAs are considered promising novel biomarkers for clinical diagnosis for example exosomal miRNAs such as miR-17, miR-19a, miR-2, miR-126 and miR-149 are highly expressed in patients with metastatic melanoma as compared to control subjects [112]. These data suggest that specific exosomal miRNAs could be involved in melanoma progression and metastasis formation and that they could be considered as predictive biomarkers of remission and relapse following therapy. Increasing evidence shows that EVs derived miRNAs can regulate proliferation of the recipient cells influencing different signalling pathway [113-115], induce chemotherapy resistance [116, 117], and reprogram glucose metabolism of cells in the pre-metastatic niche to promote metastasis [118]. It is well known that cancer-derived EV can exert important effects on endothelial cells and it was demonstrated that miRNAs can modulate angiogenesis [119] and participate in invasiveness mediating the crosstalk between metastatic cells and surrounding microenvironment thus facilitating metastasis formation [120].

CHAPTER 4: CANCER MODELS

4.1 Acute myeloid leukemia

Acute myeloid leukemia (AML) is a malignant disease of bone marrow characterized by the rapid growth of immature cells that fail to differentiate into functional myeloid cells. AML is one of the most common types of leukemia in adults. The Associazione Italiana Registro Tumouri (AIRTUM) estimates for Italy about 2000 new cases of AML every year: 1200 and 900 cases in men and women respectively (https://www.airc.it). AML is slightly more common among men than women and it is generally a disease of the elderly [121]. The only proven lifestyle-related risk factors for AML are smoking, due to the fact that cancer-causing substances in tobacco smoke are absorbed by the lungs and spread through the bloodstream to many parts of the body, and the exposure to certain chemicals like benzene, a solvent used in different industries [122]. People with certain blood disorders seem to be at increased risk of getting AML, these include chronic myeloproliferative disorders such as polycythemia vera, essential thrombocythemia, and idiopathic myelofibrosis [122]. Myelodysplastic syndrome (MDS) patients are characterized by low blood cell counts and abnormal cells in the blood and bone marrow and sometimes they can develop AML that in this case is often hard to treat [123]. No screening tests exist for AML and its diagnosis is accomplished when many signs and symptoms are already present such as the shortage of normal white blood cells (leukopenia), anemia and thrombocytopenia [124]. The subtype of AML can be important to determine prognosis. Prognostic factors include: chromosome abnormalities, gene mutations, markers on the leukemia cells, age, white blood cell counts, prior blood disorder leading to AML, treatment related to AML and status of AML after treatment [125]. Treatment of AML is usually divided into two phases. The first is called induction and it is short and intensive. The principal aim is to clear the blood of leukemia cells and to reduce the number of the blasts in the bone marrow to normal count. The second is the consolidation phase in which chemotherapy is administrated to kill leukemia cells remained after induction phase. Chemotherapy is given in cycles and each period is followed by a rest period to allow the body time to recover. In the third phase, referred as maintenance, chemotherapy is administered at a low dose for months or years after consolidation is finished [125]. The chemotherapeutic strategy usually used to treat AML is a combination of cytarabine (cytosine arabinoside or ARA-C) and anthracyclines, especially daunorubicin [126] with the so-called “3 + 7” regimen [127]. Cytarabine is a pyrimidine nucleoside analogous, it acts as an antimetabolite antineoplastic agent that inhibits the synthesis of DNA. Its action

is specific for the S phase of the cell cycle [128]. Anthracyclines are a class of drugs used in cancer chemotherapy that are extracted from *Streptomyces bacterium*. They act mainly by intercalating with DNA and interfering with DNA metabolism and RNA production by blocking the function of topoisomerase. The first anthracycline discovered was daunorubicin, which is naturally produced by *Streptomyces peucetius* [129]. Daunorubicin administration causes important side effects including hair loss, vomiting, bone marrow suppression, heart disease and tissue death at the site of injection [130]. Only 26.6% of AML patients treated with the standard combination of cytarabine and daunorubicin survived for over 5 years from 2006 to 2012 (Institute, 2016 Institute, N.C., 2016. SEER Cancer Stat Facts: Acute Myeloid Leukemia) and patients over age 60 have a poor prognosis with 10% or less 5-year survival [131] mainly due to the toxicity of therapy or disease relapse. For these reasons, new targeted drugs and strategic approaches able to reduce toxicity and to improve treatment efficacy are needed. P2X7 is highly expressed by acute myeloid leukemia cells [73] and therefore could be a potential target for AML therapy.

4.2 Melanoma

Melanoma is the most aggressive form of skin cancer and according to the World Health Organization its incidence is increasing faster than any other type of solid tumour. It usually originates in melanocytes, cells that produce the pigment melanin and it can occur in any part of the body that contains melanocytes. The main risk factors associated with melanoma are UVA and UVB radiation exposure, phenotypic characteristics like pale skin and fair hair, number of nevi and a positive family history of melanoma [132]. Melanoma is more common in males overall, but before age 50 the rates are higher in women than in men. The Associazione Italiana Registro Tumouri (AIRTUM) estimates about 7.300 and 6.700 new melanoma cases every year, among men and females respectively. The average age of people when it is diagnosed is 45-50 years, but it is not uncommon even among those younger than 30 years (Information from Associazione Italiana Ricerca sul Cancro "AIRC"). At diagnosis, a melanoma is staged based on how deeply it has grown into the skin, and whether it has spread to other parts of the body. Five different stages can be distinguished according to the American Joint Committee on Cancer:

- Stage 0: in the earliest stage, melanoma cells are localized in the epidermis
- Stage 1: melanoma is less than 1 mm thick and may or may not be ulcerated, but

there is no sign of its spreading to lymph nodes or other parts of the body. It can be easily removed by surgery.

- Stage 2: melanoma thickness is between 1.01 mm and 2 mm, it may or not be ulcerated but the risk of spreading is high. Most stage 2 melanomas can still be treated with surgery.
- Stage 3: cancer cells have spread deeper into the skin, lymph vessels or nearby glands.
- Stage 4: cancer has spread to other parts of the body, such as lung, liver, brain, bones, gastrointestinal tract, distant lymph nodes, or other areas of the skin.

If melanoma is diagnosed early it can be cured by surgical excision, with a good prognosis, while advanced stage melanomas are resistant to the most current therapies such as surgery, chemotherapy and radiotherapy, and it is associated with poor survival outcomes [133]. In 2011, the US Food and Drug Administration has approved treatments for advanced melanoma that promotes an immune response against cancer. Ipilimumab, an inhibitor of cytotoxic T-lymphocyte Associated Protein 4 (CTLA-4), was the first drug to extend the lives of patients with metastatic disease [133]. In the last eight years, a lot of novel treatments were introduced for advanced melanoma such as vemurafenib, which targets the mutant BRAF, trametinib that inhibits the kinase MEK and pembrolizumab that targets PD-1 which is expressed on T cells [133]. Immune therapy is at the moment one of the most promising therapeutic strategies to fight advanced melanoma, but unfortunately it is costly and sometimes can induce adverse effects [134]. The identification of the new molecular pathways involved in melanoma proliferation and progression will help to develop new targeted therapies for those advanced forms of the disease that don’t respond to immunotherapy. These targets can be signal transduction pathways, oncogenes, growth factors and their receptors [135]. P2X7 is expressed in human melanoma [136] and it is a potential pharmacological target as it was already demonstrated in murine models that inhibition of P2X7 prevents tumour growth and angiogenesis [54, 81]. However, the efficacy of P2X7 antagonists on cell diffusion and metastasis formation was never tested.

AIMS OF THE STUDY

The aim of this study is to investigate the role played by extracellular ATP and its receptor P2X7 in cancer progression, treatment outcomes and metastasis formation. These aspects are explored in acute myeloid leukemia (AML) and melanoma in two independent sets of experiments. ATP is a component of the tumour microenvironment in which via P2X7 can modulate tumour growth, cancer progression and immune responses. ATP can be released from dying cancer cells during a particular type of cell death named immunogenic cell death (ICD). ICD is elicited by chemotherapeutics such as anthracyclines and is associated to a specific immune response against cancer determining a favourable long-term outcome. Despite ICD was already demonstrated in AML, the effect of anthracyclines on ATP release was never investigated in this oncologic model. Thus, we studied the effect of daunorubicin and cytarabine, which are known respectively to induce or not ICD, on ATP release and induction of immune response in an *in vivo* AML model. Moreover, it was demonstrated that in AML P2X7 is expressed exclusively by transformed leukemic blasts and not by healthy CD34 counterpart suggesting a correlation between P2X7 and AML onset and progression. Among the ten splice variants of the receptor, only P2X7A and P2X7B are functional channels in human showing a growth promoting activity. However, P2X7B differs from P2X7A for the inability to form the cytotoxic large pore in presence of high ATP concentration. We correlated the expression of the two P2X7 isoforms with the progression of the disease and with response to chemotherapy in a cohort of patients affected by myelodisplastic syndrome, a pre-cancerous condition leading to AML development, and by AML. We then investigated the differential effect of daunorubicin treatment on cells expressing P2X7A or P2X7B.

Advanced forms of melanoma are still a clinical challenge for clinicians as they are mostly refractory to current treatments. Thus, new targeted drugs and therapy strategies are needed. In an effort to identify whether P2X7 could be a novel pharmacological target in melanoma therapy, we correlated P2X7 expression with melanoma agressiveness on a cohort of metastatic melanoma patients. We investigated the effect of P2X7 antagonists on primary tumour growth and metastasis diffusion on the ATP content of the TME and nature of tumour infiltrating immune cells. Finally, to better understand whether P2X7 can influence melanoma spreading we analysed vesicles release from melanoma cells, a mechanism of cell communication that partecipates in tumour colonization of distant tissues and preparing the pre-metastatic niche.

MATERIAL AND METHODS

Cell cultures

WEHI-3B myelomonocytic murine leukemia cells, HL60 human promyelocytic cells, B16 melanoma cells and HEK293 human embryonic kidney cells stably expressing P2X7A, P2X7B or empty vectors were previously available at Adinolfi laboratory [40, 54, 80, 81]. Human melanoma cell lines A-2058, GR-M, A-375, Ma-Mel-19, and Sk-Mel-28 were purchased from the European Collection of Authenticated Cell Cultures (ECACC). Screening of Mycoplasma contamination was periodically conducted with MycoAlert™ Mycoplasma Detection Kit (Lonza). HL-60 and all melanoma cell lines were cultured in RPMI-1640 medium (Sigma-Aldrich, Saint Louis, Missouri, USA), HEK 293 cells were cultured in DMEM High Glucose medium (Sigma-Aldrich) while WEHI-3B cells were cultured in Iscove's Modified Dulbecco's Medium (Sigma-Aldrich), all supplemented with 10% foetal bovine serum (FBS) (Euroclone, Milan, Italy), 100 U/ml penicillin (Euroclone), and 100 mg/ml streptomycin (Euroclone) at 37°C and 5% CO_2. To maintain the expression of P2X7A, P2X7B and empty vectors on HEK293 cells selection with neomycin/G418 sulfate (0,4 mg/ml) (Sigma-Aldrich) for HEK P2X7A expressing cells, with Hygromycin B (0,2 mg/ml) (Sigma-Aldrich) for HEK P2X7B expressing clones or both for mock clones was added once a week to the growing cells as previously reported [40, 45].

Cell transfections

To obtain B16 and WEHI-3B cell clones stably expressing plasma membrane luciferase pmeLUC, cells were transfected with the pmeLUC expression vector, as described in [20]. B16 cells were transfected with Lipofectamine LTX (Thermo Fisher Scientific, Waltham, Massachusetts, USA), as reported in the manufacturer's instructions, while WEHI-3B were electroporated as follows: 6 $x10^6$ cells were suspended in electroporation buffer (Thermo Fisher Scientific) with 3 µg of plasmid's DNA and electroporated in a Microporator MP-100 (Digital bio, Thermo Fisher), at 1,250 V for 40 ms. Stably transfected cell clones were obtained by selection with neomycin/G418 sulfate (0.4 mg/mL; Sigma-Aldrich) followed by limiting dilution as previously described [54]. To obtain Sk-Mel-28 cell clones stably expressing cytoplasmic luciferase, cells were transfected with the Luc2 probe using Lipofectamine LTX in the presence of 3 µg plasmid's DNA as per manufacturer's instructions and transfected clones were obtained by selection with hygromycin B (0.2 mg/mL; Sigma-Aldrich).

Mice strains, tumour generation and drugs administration

In vivo experiments were performed using athymic nude-Foxn1nu, BALBc/J and C57bl/6 mouse strains. To obtain palpable tumours, cells were subcutaneously injected and tumour size was measured with a calliper, and volume calculated according to the following equation: $\pi/6$ [ω_1 x $(\omega_2)^2$], were ω_1 is the major diameter and ω_2 is the minor diameter. To obtain experimental metastasis cells were injected into the tail vein of mice. $2X10^6$ WEHI-3B pmeLUC cells were subcutaneously injected into male 4-6 weeks old BALB/cJ. Daunorubicin (DNR) (3 mg/kg, Sigma), cytarabine (ARA-C) (50 mg/kg, Sigma), or sterile PBS vehicle (placebo) were i.p. administered at p.i. days 7 and 9 and mice sacrificed on day 12. Luminescence emission was measured every day, from day 7 to 12. 4-6 weeks old female animals were subcutaneously injected with 5×10^6 HL-60 (Athymic nude) and received intra-mass injections of sterile PBS (placebo), daunorubicin (150 μg/ml), P2X7 antagonist AZ10606120 (2 μM) or both compounds at post-inoculum days 8 and 10. Tumour size was measured at post-inoculum days 8, 10 and 12 and *ex vivo*. $2.5x10^5$ B16 pmeLUC were subcutaneously injected into C57bl/6 4-6 weeks old female mice. P2X7 antagonist A740003 (50 mg/kg) (Tocris Bioscience, Bristol, UK) or vehicle (PBS, 0.005%DMSO) were intra-peritoneum injected every 2 days after day 5, corresponding to first tumour mass detection and mice sacrificed at day 14. Luminescence emission was measured every other day, from day 5 to 14. $1x10^6$ Sk-Mel-28 Luc 2 cells were injected into the tail vein of 4-6 weeks old female Athymic nude mice. Luminescence emission measurement and intra-peritoneum injection of P2X7 antagonist A740003 (50 mg/kg) or vehicle (PBS, 0.005% DMSO) were performed every 72 hours for 45 days. At the end of the experiments, whenever required blood was collected before sacrifice the animals and tumours were excised and processed for further analysis. All animal procedures were approved by the University of Ferrara Ethics committee and the Italian Ministry of Health in compliance with international laws and policies (EU Directive 2010/63/EU and Italian D.Lgs 26/204).

Processing of *ex vivo* samples

Blood samples were collected from the submandibular vein under general anesthesia immediately before sacrifice the animal. Mouse plasma was collected by centrifugation (1000 x *g*, 10 min at 4°C) of blood and stored at – 80°C in the presence of Halt Protease and Phosphatases Inhibitor Cocktail, EDTA-Free (Thermo Fisher Scientific). For RNA extraction, tumours were lysed with TRIZOL (Ambion, Life Technologies) plus 4% 2-

Mercaptoethanol (BIORAD). After homogenization by electric tissue homogenizer (VWR International Srl, Milano, Italy) samples were passed 5 times through the 18-21 gauge needle of an RNase-free syringe and then centrifuged at 12000 x g for 2 minutes. An equal volume of 70% ethanol was added to the supernatants collected and total RNA was extracted using the PureLink RNA Mini Kit (Thermo Scientific, Milano, Italia).

In vivo luminescence emission measure

Luminescence emission was measured with a total body luminometer for small animals (IVIS Lumina, Calliper; Perkin Elmer, USA), as described in [20]. Mice anesthetized with 2.5% isofluorane were intra-peritoneum (i.p.) injected with 150 mg/kg D-luciferin (Promega, USA) and luminescence was captured from dorsal (for pmeLUC cells) and ventral (for Luc2 cells) views. Photon emission was quantified using the Living Image® software (Perkin Elmer) as total photons/seconds (abbreviated as p/s) or averaged as photons/seconds/cm^2/steradian (abbreviated as p/s/cm^2/s).

Cytokines evaluation

Cytokines levels were evaluated following 1:2 plasma dilution either with Mouse IL-1β, IL-2, IL-12 (Boster, distributed by Tema Ricerca, Bologna, Italy), IFN-γ (R&D, Bio-techne) ELISA kits or with Ciraplex CK1 mouse multi-cytokine assay kit (Aushon Biosystem, distributed by Tema Ricerca, Bologna, Italy) as per the manufacturer's instructions.

Clinical samples

Primary leukemic cells were obtained, as previously described [137], from the peripheral blood (PB) or bone marrow (BM) of 93 patients subdivided according to diagnostic phase in: 16 myelodysplastic syndrome (SDM), 61 first diagnosed of acute myeloid leukemia (*de novo* AML), 11 with relapse of the disease after chemotherapy and 5 remitting AML patients. These samples were used for RNA extraction. Samples from human melanoma patients were obtained from two commercial arrays (TissueScan Melanoma Tissue qPCR Panel I MERT 01 and MERT 02, OriGene Technologies). Melanoma samples are subdivided according to the diagnostic stage and site of metastasis in four groups: stage III (n=19), stage IV with skin metastasis (n=15), stage IV with lung metastasis (n=12) and stage IV with metastasis in other distant organs including brain and liver (n=14). A panel of 57 different melanoma specimens from 20 females and 37 males, among which 15

metastatic melanomas, was analyzed using tissue array slides CK2-D human Super Bio chips (Super Biochips, South Korea distributed by Tema Ricerca, Bologna, Italy).

Real-Time quantitative RT-PCR

Total RNA was extracted using PureLink RNA Mini Kit (Thermo Scientific, Milano, Italia) and RNA content was determined with a Nanodrop 2000 spectrophotometer (Thermo Scientific). mRNA reverse transcription to cDNA was performed with the High-Capacity cDNA Reverse Transcription Kit (Applied Biosystems) using 200 ng of RNA/sample as a template. The mRNA was retro-transcribed in a Biometra UNO-Thermoblock (DASIT, Milan, Italy) with the following thermal conditions: 25°C for 10 min; 37°C for 120 min; 85°C for 5 min. 2µl of the obtained cDNA was used as a template for Real-Time quantitative RT-PCR (qRT-PCR) using TaqMan® MGB probes, FAM™ dye-labeled (60X) and TaqMan Gene Expression Master Mix (2X) in a final reaction volume of 20 µl (Thermo Fisher Scientific). qRT-PCR was performed thanks to an AB PRISM 7300 Step One Real-Time PCR system (Applied Biosystems): holding stage 50°C/2 min; 95°C/10 min following by cycling stage: 95°C/15 sec; 60°C/1 min for a total of 40 cycles. Amplification was performed with Taqman probes (Applied Biosystem) for P2X7A, P2X7B, and GAPDH as reference mRNA. Pre-designed and custom primers were those previously described by [40]. A comparative CT experiment (ΔΔCT) was run to allow determination of the change of expression (fold increase) of the target cDNA in the test sample relative to the Te85 cell line reference sample, which was previously demonstrated to express minimal levels of both P2X7A and B [45].

Measurement of intracellular calcium concentration with FURA-2AM

The activity of P2X7 as Ca^{2+} channel was measured by assessing the cytosolic free ion concentration in a thermostat-controlled (37°C) and magnetically stirred Cary Eclipse Fluorescence Spectrophotometer (Agilent Technologies, Milan, Italy) with the fluorescent dye FURA-2/acetoxymethyl ester (FURA-2/AM, Molecular probes, Life Technologies). Briefly, 2×10^6 cells were loaded in standard saline solution with 2 µM FURA-2/AM plus 250 µM sulfinpyrazone for 25 min, rinsed, and resuspended at a final concentration of 2 $x10^6$/ml in the same buffer. Excitation ratio and emission wavelengths were 340/380 and 505 nm, respectively.

Measurement of plasma membrane permeabilization to ethidium bromide

Increases in ethidium bromide uptake were measured in a Cary Eclipse Fluorescence Spectrophotometer (Agilent Technologies). 1×10^6 cells were re-suspended in standard buffer (see above), incubated in the presence of 20 μM ethidium bromide at 37°C and under magnetical stirring. After approximately 2 minutes cells were challenged with P2X7 agonist BZ-ATP (500 μM) or daunorubicin (200 nM). Full permeabilization was obtained with 100 μM digitonin. Fluorescence emission was measured at an excitation/emission wavelength of 360/580 nm.

Cells viability assays

HEK293 MOCK, -P2X7A, -P2X7B were resuspended in DMEM High Glucose (Sigma-Aldrich) serum-free medium, seeded at a concentration of 2 $x10^5$ in 6-well plates (Euroclone) and maintained in an incubator at 37°C and 5% CO_2. Cells were treated with PBS or 200 nM daunorubicin for 48 hours. Ma-Mel-19 and Sk-Mel-28 cells were seeded at a concentration of 3 $x10^4$ in 6-well plates and maintained in an incubator at 37°C and 5% CO_2. Cells were treated with vehicle (PBS/DMSO), 20μm A740003 or AZ10606120 for 48 hours. In both experiments cell number was assessed at time 0, 24 and 48 hours by acquiring 5 photographs per well with a 40x/0,5 magnification (Leica) with a DM IL Led Leica Microsystem (GmbH) microscope (LEICA ICC50 HD) and counting thanks to the ImageJ 1.42I software (Wayne Rasband, NIH, Bethesda, MD). For HEK293 cell viability was also assessed with the AlamarBlue Cell Viability Reagent (Thermo SCIENTIFIC) as described by manufacturers. Briefly, 20.000 cells were plated at 100μL/well in a 96-well plate and incubated overnight at 37°C, 5% CO_2. Cells were treated with PBS or 200 nM daunorubicin for 24 hours. The alamarBlue Reagent (10μL/well) was then added and cells absorbance was measured after 4 hours of incubation at 37°C, 5% CO_2 at $545nm_{Ex}/590nm_{Em}$ using a plate reader Perkin Elmer Wallac Victor3 1420 luminometer (Perkin Elmer, Wellesley, Massachusetts, USA).

Daunorubicin permeabilization assays

HEK293 MOCK, -P2X7A, -P2X7B were resuspended in DMEM High Glucose (Sigma-Aldrich), seeded at a concentration of $2x10^4$ on 40 mm diameter glass coverslip (VWR International Srl) and maintained in a Sanyo incubator at 37°C and 5% CO_2. All experiments were set up in standard saline solution with the addition of daunorubicin 1 μg/ml, maintained in a thermostated Leyden chamber (mod. TC-202, Medical Systems Corporation, NY) at 37°C located on a Nikon Eclipse TE300 inverted microscope. Cells

were imaged by means of $328nm_{EX}/545nm_{Em}$ filters on a CCD camera (Photometrics ® Coolsnap EZ) equipped with a 20x/0,45 objective (ELWD, Nikon, Japan). Cells images were sequentially acquired every 30 seconds for 91 stocks. Images were then analyzed with Metamorph software ® (Universal Imaging Corporation, West Chester, PA, USA). $5x10^4$ HL60 cells were resuspended in RPMI complete medium and all experiments were set up in standard saline solution with the addition of daunorubicin 1µg/ml in 6-well plate. Cells were then stimulated or not with 3mM ATP and images were acquired every 15 minutes for a total of 45 minutes with a Leica DMI 4000B (Leica Microsystems CMS GmbH) microscope. Images were acquired both in bright field and in fluorescence ($328nm_{EX}/545nm_{Em}$) thanks to a Leica DFC 550 camera equipped with a 20x/0,55 objective (Leica).

***In vitro* measure of ATP levels**

ATP was measured in the culture supernatants with ENLITEN rLuciferase/Luciferin reagent (Promega), as per the manufacturer's instructions. In the first case, $5 x10^5$ HL-60 cells were treated for 24 hours with vehicle (PBS), daunorubicin (200 nM), AZ10606120 (2 µM) or both compounds. Supernatants were collected after a 5 minutes centrifugation at 900 rpm and 100 µl per sample was mixed with an equal volume of ENLITEN reagent allowing for the measure of luminescence. In the second case, $5 x10^4$ B16 cells and peritoneal macrophages per well were plated in six-well plates. Following adhesion cells were incubated for 48 hours in the presence of a vehicle or A740003 20 µM (Tocris Bioscience), corresponding to *in vivo* administered concentration. In both cases, luminescence from cell supernatants was measured following the addition of 100 µl of ENLITEN reagent per well, in a Perkin Elmer Wallac Victor3 1420 luminometer (Perkin Elmer, Wellesley, Massachusetts, USA). A standard curve obtained with known concentrations of ATP allowed an estimate of the molar concentration of the nucleotide in the supernatants.

Immune cells isolation and co-culture conditions

Macrophages were recovered from C57bl/6 mice by peritoneal lavage as described previously [138]. Briefly, the peritoneal cavity was lavaged with ten 1ml aliquots of sterile PBS (pH 7.4), and cells were harvested by centrifugation at 200 x g at 4° C for 5 minutes. Macrophages were co-cultured with HLA-matched pmeLUC expressing tumour B16 cells with a ratio of 1:1. Supernatant ATP levels were determined with the ENLITEN kit while

tumour cell surrounding ATP was assessed by pmeLUC luminescence measure as above described.

Evaluation of the tumour-immune infiltrate by flow cytometry

Tumour-infiltrating lymphocytes and dendritic cells were characterized on tumour cell suspension after separation by Ficoll gradient (GE Healthcare Life Sciences, Little Chalfont, Buckinghamshire, UK). For the staining of surface markers, tumour-infiltrating lymphocytes and dendritic cells were incubated for 30 minutes at 4°C in the dark with the following anti-mouse mAbs: CD39-PE (clone DUHA59; BioLegend) and CD73-BV605 (clone 7Y/11.8; BioLegend) according to the manufacture's instruction. Flow cytometry data were acquired on an LSRFortessa (Becton Dickinson, Franklin Lakes, New Jersey, USA) and analyzed with FlowJo software (version 8.8.7, Tree Star Inc.) from tumour mass by Ficoll (GE Healthcare Life Science) gradient.

Immunohistochemistry

Slides were heated at 60°C for 20 minutes, deparaffinized with xylene and rehydrated by sequential passages through decreasing concentrations of ethanol. Endogenous peroxidase activity was blocked by 15 minutes incubation at room temperature with 0.3% H_2O_2 in TBS (50 mM Tris, 150 mM NaCl, pH 7,6). After three rinses in wash buffer (0.025% Triton X-100 in TBS), tissue sections were maintained for 2 hours at room temperature with a blocking solution (1% BSA, 10% FBS in TBS), and incubated overnight at 4°C with a rabbit polyclonal anti-P2X7 antibody (P8232, Sigma) (20 µg/ml) in incubation solution (1% BSA in TBS). Sections were rinsed twice in wash buffer, incubated for 60 minutes at room temperature with appropriated HRP conjugated secondary antibodies (goat anti-rabbit) diluted 1:100 in incubation solution, washed in TBS, and submitted to 6-10 minutes incubation at room temperature with Liquid diaminobenzidine (DAB) Substrate Chromogen System (Dako). Counterstaining was performed with Mayer's hematoxylin. Images were acquired with a Nikon Eclipse H550L microscope (Nikon) using the NIS-Elements software (Nikon).

Soft agar colony formation assay

A cell suspension ($5x10^4$ cells per well) was mixed with 0.8% agar solution and with either P2X7 antagonists (A740003 20 µM and AZ10606120 2µM) or the vehicle (PBS). This mixture was seeded into a 6-well plate covered by a layer of solidified agar previously prepared with 0.6% agar mixed with RPMI-1640 culture medium. The plate was placed

into a 37°C humidified cell culture incubator and allowed to form colonies. Images of all wells were taken with a phase-contrast optical microscope after 20 days and colonies were counted by the operator.

Scratch recovery assay

The scratch recovery assay is one of the common *in vitro* assays used to determine the migratory behavior of cells. The rate of recovery of the scratch is indicative of the metastatic potential of cells *in vivo*. Sk-Mel-28 and Ma-Mel-19 cells were cultured in 6-well multi-well. When cells were grown at confluence, a scratch was manually made with a sterile 200 µl pipette tip in a marked region of the plate. Cells were washed to remove displaced and floating cells. Images of the scratches were obtained at Time 0 (T0) and after 24 and 48 hours (T24, T48) with a phase-contrast optical DM IL Led Leica Microsystem (GmbH) microscope (LEICA ICC50 HD). Image analysis was performed using ImageJ software to evaluate the rate of recovery of the scratch.

Large and small vesicles isolation

Large and small vesicles were isolated from cell culture supernatant by differential ultracentrifugation. Cells were incubated for 30 minutes with or without 3 mM ATP at 80% confluence in saline solution at 37°C with 5% CO_2. In order to obtain vesicle fractionation, the supernatant was first depleted of cells and debris by centrifuging at 2000 x g for 20 minutes at 4°C. Large vesicles enriched fraction was then pelleted at 18 000 x g for 40 minutes at 4°C. To collect small vesicles, the supernatant depleted of larger vesicles was centrifuged at 100 000 x g for 4 hours at 4°C. Both fractions were washed in phosphate-buffered saline (PBS).

Optical and electron microscopy analysis

Sk-Mel-28 and Ma-Mel-19 cells were detached from the flask by using cell dissociation solution and then plated 2 $x10^4$ onto 40-mm glass coverslips (Thermo Scientific). Experiments were performed in standard saline solution (125 mM NaCl, 5 mM KCl, 1 mM $MgSO_4$, 1 mM NaH_2PO_4, 20 mM HEPES, 5,5 mM glucose, 5 mM $NaHCO_3$, 1 mM $CaCl_2$, pH 7,4) and cells were treated with 3 mM ATP. Morphological changes and vesicles shedding were analyzed by mounting coverslips on a thermostatted Leyden chamber (model TC-202A; Medical Systems Corp., NY, USA), placed onto the stage of an inverted Nikon Eclipse TE300 microscope (Nikon Corp., Tokyo, Japan). The images were captured with a black-illuminated CCD camera (Princeton Instruments, Trenton, NJ, USA) using the

Metamorph software (Universal Imaging Corporation, West Chester, PA). For electron microscopy analysis, Sk-Mel-28 and Ma-Mel-19 cells were incubated with saline solution for 10 minutes with 3 mM ATP or without ATP, then they were detached from the flasks with 2 mM EDTA-containing cold PBS, centrifugated at 1100 rpm for 5 minutes and cell pellets were fixed with 2.5% glutaraldehyde. Samples for electron microscopy were processed by the Centro di Microscopia Elettronica of the University of Ferrara (Ferrara, Italy).

Nanoparticle Tracking Analysis (NTA)

Purified large and small vesicles were resuspended in 60 µl of PBS and diluted 1:100 in particles free PBS to an acceptable concentration. According to the manufacturer's software manual (Nanosight LM10, Malvern, UK), the camera level was increased until all particles were distinctly visible and the ideal detection threshold was determined to include as many particles as possible (15 particles/frame). For each measurement, five 1 minute videos were captured under the following conditions: temperature 25.6-25.7°C, syringe speed 30 µl/s. After capture, the videos have been analyzed by the in-build NanoSight Software NTA 3.2 Dev Build 3.2.16 with a detection threshold of 5, laser type Blue488 and camera type sCMOS.

NGS sequencing

RNA was extracted from vesicles collected in QIazol Lysis Reagent using the miRNeasy®Mini Kit (Qiagen) following manufacturer's instructions. Small RNA sequencing was performed using the QIAseq miRNA library kit (Qiagen) and Illumina NextSeq500 sequencer (Illumina). A total of 2553 microRNAs were analyzed. Raw data were proceeded by Qiagen GeneGlobe Data Analysis Center to obtain miRNA quantification, with Unique Molecular Indices (UMIs) correction for potential PCR and sequencing bias. DESEQ2 normalized data were imported in GeneSpring software (Agilent Technologies) for data analysis. A 1.5 fold change filter and $p<0.05$ at moderated t-test for group comparison were used.

Statistics

All data are shown as mean ± standard error of the mean (SEM). Significance was calculated assuming equal SD and variance, with a two-tailed Student's *t*-test performed with the GraphPad Prism software (GraphPad, La Jolla, California, USA). *P*-values lower than 0.05 were considered statistically significant.

RESULTS CHAPTER I

Role of extracellular ATP in acute myeloid leukemia and P2X7 receptor in chemotherapy resistance

ATP levels are increased in the tumour microenvironment of daunorubicin treated leukemia bearing mice.

We investigated the effect of chemotherapeutics daunorubicin and cytarabine on ATP levels in the tumour microenvironment. To obtain an *in vivo* model of acute myeloid leukemia (AML) murine WEHI-3B AML cells transfected with pmeLUC, a luciferase expressed at the plasma membrane which allows for ATP measure in the extracellular milieu were subcutaneously injected in syngeneic BALB/cJ mice. Mice were then treated with placebo (PBS) (100 µl), daunorubicin (DNR) (3 mg/kg), or cytarabine (ARA-C) (50 mg/kg) at post inoculum days 7 and 9. We observed that while DNR and ARA-C treatment had comparable effect on tumour mass reduction (Figure 1A) only DNR induced a significant increase in ATP release (36,094.20 ± 7,420.75 p/s/cm^2/sr) over control (13,950.9 ± 4,118.65 p/s/cm^2/sr) (Figure 1B) at days 11 and 12.

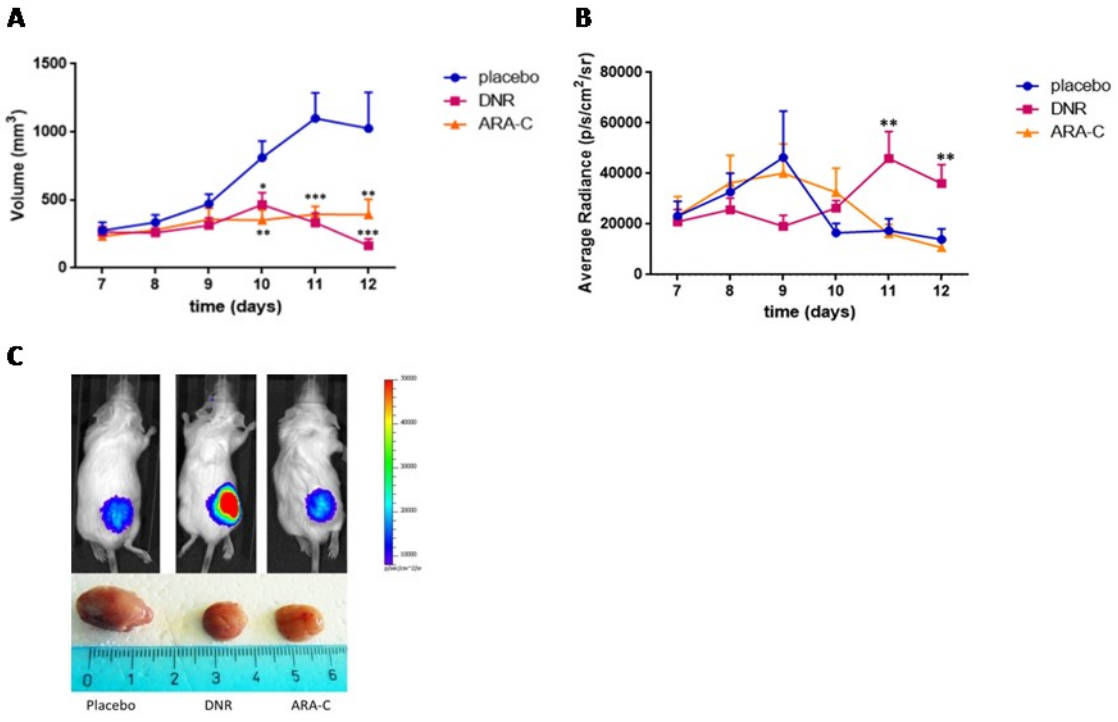

Figure 1 Daunorubicin increases ATP release *in vivo* model of AML

BALB/cJ mice were subcutaneously injected with WEHI-3B pmeLUC cells and treated with DNR (3 mg/kg), ARA-C (50 mg/kg), or placebo (PBS, 100 µL) at post-inoculum days 7 and 9. **(A)** Tumour volume

was *in vivo* assessed every day from post-inoculum day 7. **(B)** Measure of ATP in treated BALB/cJ mice estimated by pmeLUC luminescence. Data are presented as the average number of photons in the tumour microenvironment (p/s/cm^2/steradian). Data are shown as the mean ± SEM of 12 mice per condition. *p<0.05, **p<0.01, ***p<0.001 versus placebo. **(C)** Representative pictures of pmeLUC luminescence emission in treated BALB/cJ mice and of *ex vivo* tumour volumes at post-inoculum day 12.

Daunorubicin treatment increases circulating pro-inflammatory cytokines

To investigate if ATP released following daunorubicin treatment induces a tumour eradicating immune response, we analysed the levels of the main cytokines correlated to immunogenic cell death in mice serum by ELISA. We observed that administration of DNR but not ARA-C promoted a significant increase of the pro-inflammatory cytokines IFN-γ, IL-1β, IL-2 and IL-12 in the serum of leukemia-bearing mice.

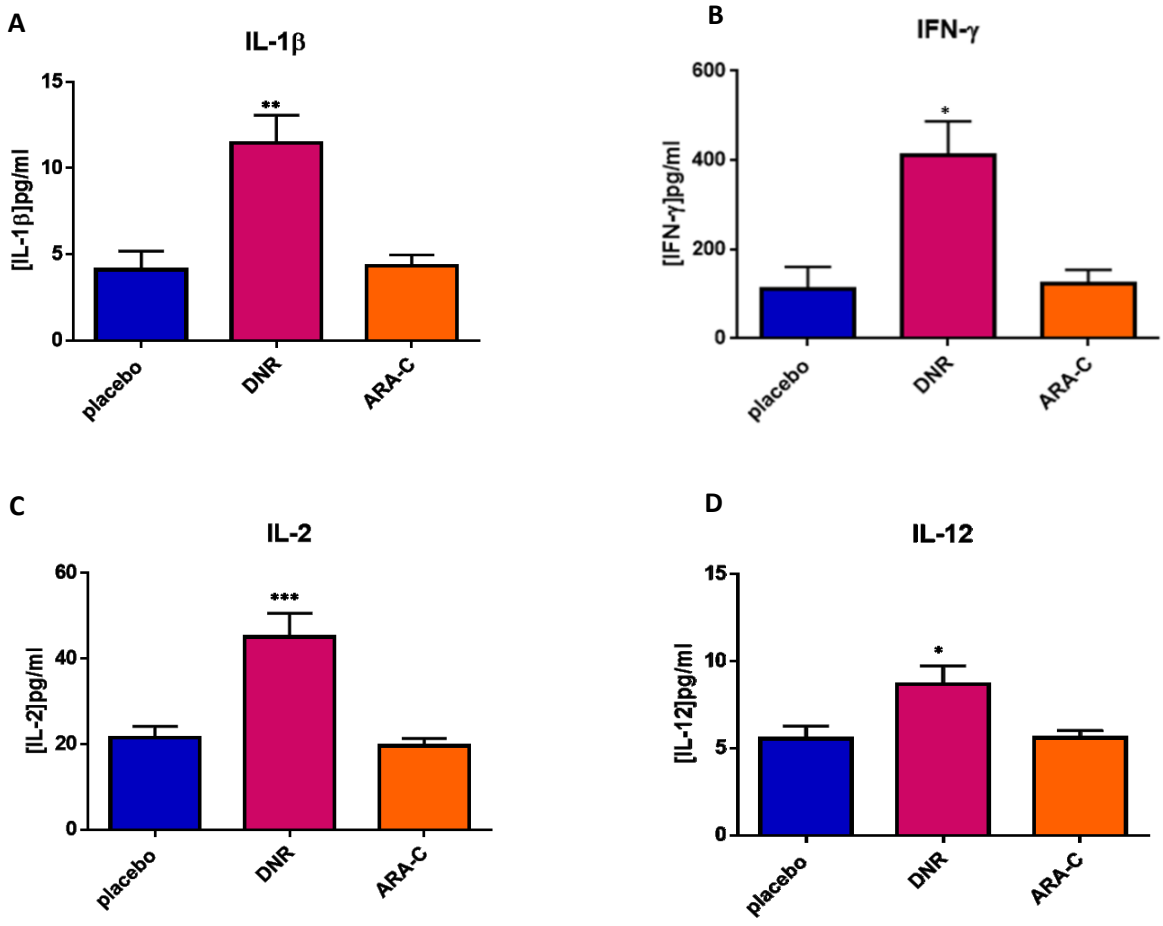

Figure 2 Daunorubicin increases the serum levels of pro-inflammatory cytokines

Levels of the pro-inflammatory cytokines IL-1β (**A**), IFN-γ (**B**), IL-2 (**C**) and IL-12 (**D**) in serum at post-inoculum day 12 of mice inoculated with leukemic WEHI-3B pmeLUC cells and treated with DNR (3 mg/kg), ARA-C (50 mg/kg), or placebo (PBS). Data are shown as the mean ± SEM of 12 mice per condition. *p<0.05, **p<0.01 and ***p<0.001 versus placebo.

To extend the findings obtained in the animal model tested to a patient's population we investigated P2X7 expression in an AML cohort.

P2X7A and P2X7B are highly expressed in newly diagnosed acute myeloid leukemia compared to myelodysplastic syndrome

P2X7 expression was already demonstrated in AML [73], but the differential expression of the P2X7A and P2X7B isoforms was never related to disease progression and response to chemotherapy. Therefore, we investigated by Real-Time PCR mRNA levels of P2X7A and P2X7B in a cohort of patients in which 16 were affected by myelodysplastic syndrome (MDS), a pre-cancerous condition often leading to AML development, and 61 affected by AML. Both P2X7A and P2X7B are highly expressed in AML *de novo* patients as compared to MDS.

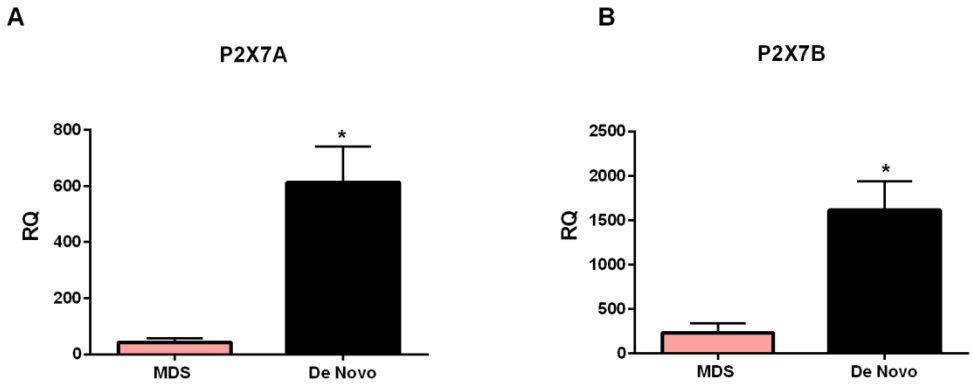

Figure 3 Both P2X7A and P2X7B are highly expressed in *de novo* AML patients as compared to MDS patients. Real Time PCR analysis of P2X7A **(A)** and P2X7B **(B)** mRNA levels from bone marrow of *de novo* (n=61) and MDS patients (n=16)**.** *p<0.05

P2X7A and P2X7B are differentially regulated in relapsing patients

AML patients were subdivided according to diagnostic phase into three groups: newly diagnosed untreated AML (*de novo*, n=61), relapsing patients with a return of the pathology after chemotherapy (relapsing, n=11) and remitting patients (remitting= 5). We compared the expression of P2X7 isoforms A and B in the three different AML groups. Interestingly, relapsing patients show a significant decrease in P2X7A expression (Figure 4A) and a significant increase of P2X7B levels (Figure 4B) as compared to *de novo* patients, suggesting that chemotherapy can cause a positive selection of cells expressing P2X7B and induce death of those expressing P2X7A. On the contrary, in remitting patients both P2X7A and P2X7B levels significantly decreased as compared to *de novo* patients

(Figure 4A-4B). These data suggest that subjects expressing high levels of P2X7B could be resistant to chemotherapy and predisposed to relapse. Therefore, P2X7B is a potential progression biomarker for AML.

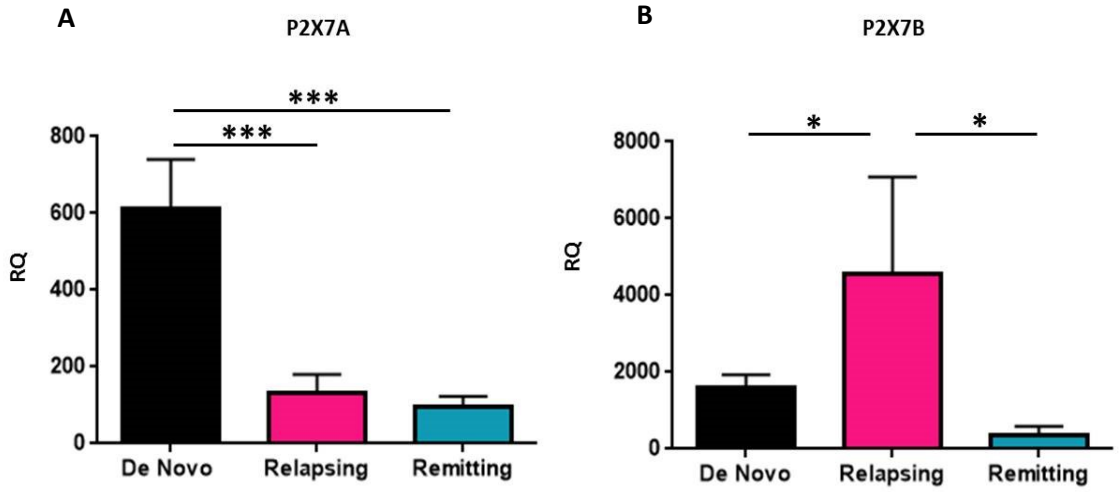

Figure 4 P2X7A and B are differentially regulated in relapsing patients. Real-Time PCR analysis of P2X7A and P2X7B mRNA extracted from bone marrow. Comparison of P2X7A (**A**) and P2X7B (**B**) levels among *de novo* (n=61), relapsing (n=11) and remitting patients (n=5). *p<0.05, ***p<0.001

All patients experiencing a relapse in AML were treated with daunorubicin. Therefore, we hypothesis that extracellular ATP released following daunorubicin administration could kill blasts overexpressing P2X7A while it will promote proliferation of P2X7B expressing leukemic cells (Figure 5). This hypothesis was tested in *in vitro* and *in vivo* AML experimental models.

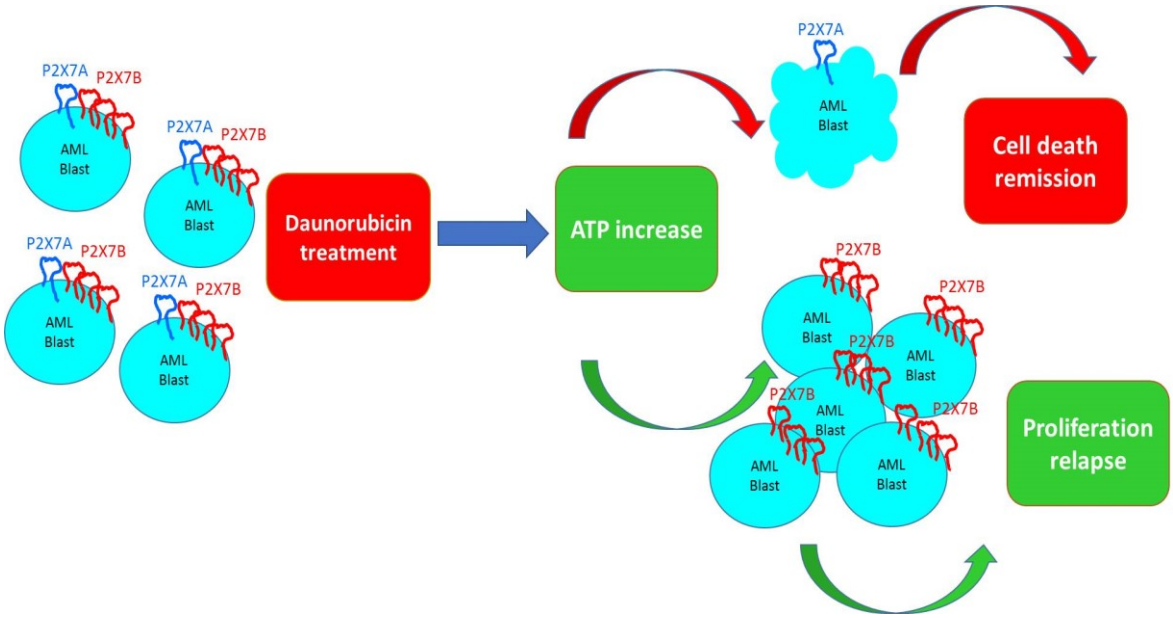

Figure 5 Proposed model: ATP responsible for positive versus negative selection of P2X7 isoforms in AML. Daunorubicin treatment induces ATP release in the tumour microenvironment. P2X7A expressed by AML blasts in the presence of high ATP concentration undergoes a channel to pore transition triggering cell death. P2X7B expressed by AML blasts and activated by ATP is unable to form the cytotoxic pore but retains the growth-promoting activity of the channel favouring leukemia relapse.

HL60 human leukemia cells express P2X7A and B isoforms and release ATP following daunorubicin treatment.

To study the role of P2X7 isoforms in AML we took advantage of the HL-60 human promyelocytic cell line that expresses both P2X7 isoforms at the mRNA level (Figure 6A-6B) and a receptor functional as both ion channel (Figure 6C) and large solutes pore (Figure 6D). Treatment with daunorubicin increased ATP release from HL-60 cells and this effect was even incremented by co-treatment with P2X7 antagonist AZ10606120 (Figure 6F).

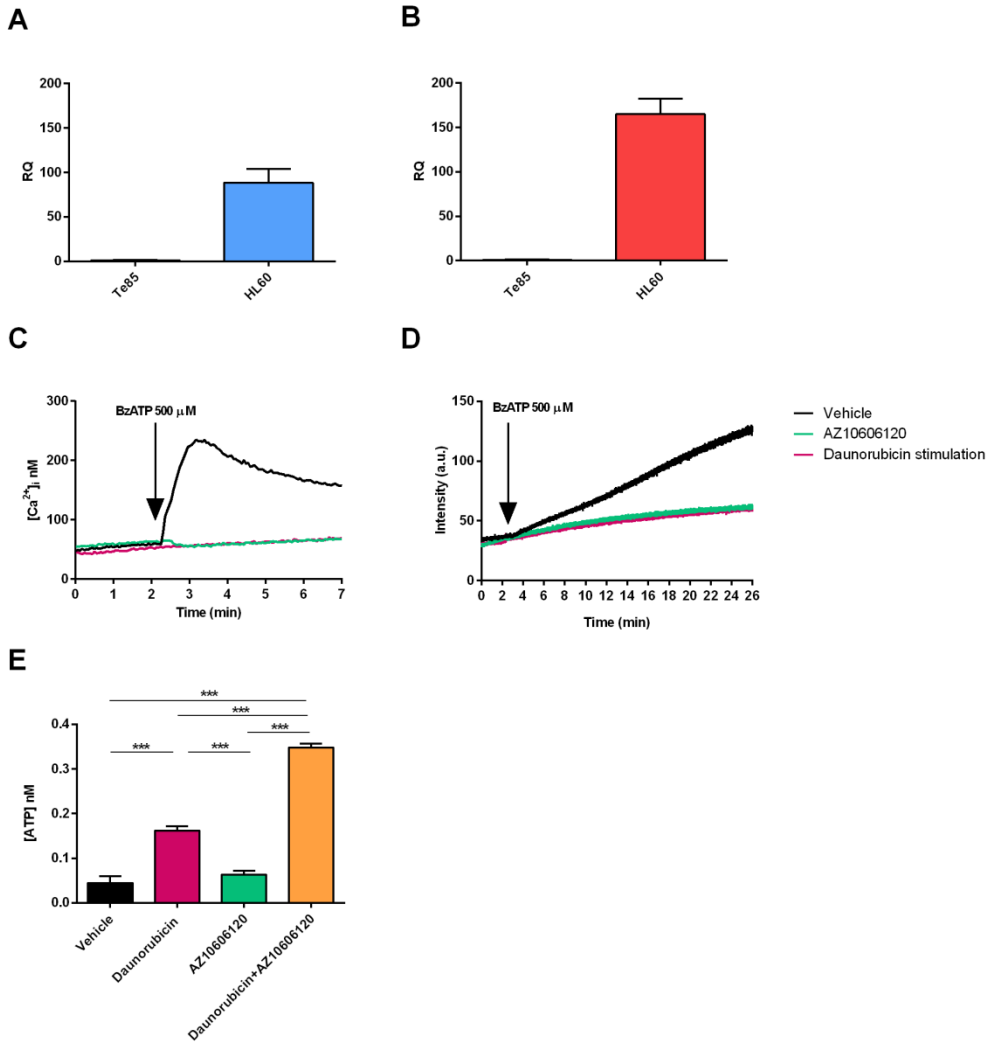

Figure 6 HL-60 cell line expresses both P2X7A and P2X7B and releases ATP following daunorubicin treatment. mRNA expression of P2X7A (**A**) and P2X7B (**B**) in HL-60 cells was evaluated by Real Time-PCR using Te85 cells as a reference sample. (**C** and **D**) HL-60 cells were treated with a vehicle (PBS) and P2X7 antagonist AZ10606120 (2 µM) and stimulated with BzATP (500 µM) or stimulated with daunorubicin (200 nM). Functional activity of the P2X7 receptor as a channel (**C**) was evaluated measuring variations in $[Ca^{2+}]i$ or as a pore (**D**) was evaluated measuring ethidium uptake. (**E**) Measure of ATP concentration in the supernatant of HL-60 cells treated with vehicle (PBS), daunorubicin (200 nM), P2X7 antagonist AZ10606120 (2 µM) or both compounds. *p< 0.05, ***p<0.001

***In vivo* co-administration of daunorubicin and P2X7 antagonist AZ10606120 is more efficacious in reducing tumour growth than the single drugs.**

In an effort to reproduce an *in vivo* murine model of AML we subcutaneously injected HL-60 cells in athymic nude mice. Tumours were treated with intra-mass injections of placebo (PBS, 100 µl), daunorubicin (1 mM), AZ10606120 (2 µM) or both compounds together. Both drugs significantly reduced leukemia growth, but their co-administration was more efficacious than the single drug administration (Figure 7A). Daunorubicin effect on P2X7 isoforms expression was similar to patients' data as P2X7B expression was significantly increased by daunorubicin (Figure 7D) while P2X7A showed a tendency to reduction (Figure 7C). Interestingly, the co-administration of daunorubicin with AZ10606120 normalized both P2X7A and B levels.

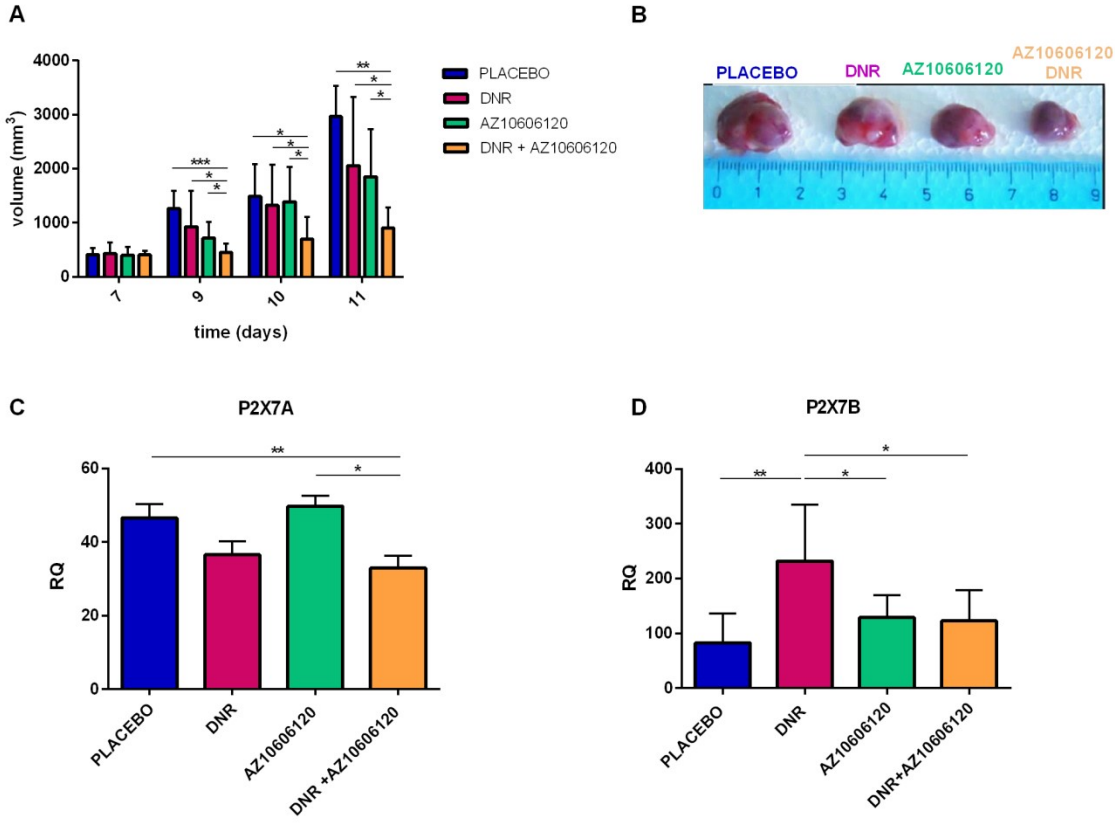

Figure 7 Co-administration of daunorubicin and AZ10606120 is more efficacious to reduce tumour growth than the single drug administration. Athymic nude mice were inoculated into the right hind flank with HL-60 cells. Mice were treated with intra-mass injections of placebo (PBS, 100 µl), daunorubicin (1 mM), AZ10606120 (2 µM) or both compounds at post-inoculum days 7 and 10. (**A**) Tumour volume was *in vivo* and *ex vivo* assessed by a calliper. (**B**) Representative picture of tumours from treated mice. Real-time PCR analysis of P2X7A (**C**) and P2X7B (**D**) mRNA extracted from homogenized tumours. Data are shown as the mean ± SEM of 7 mice per condition *p<0.05, **p<0.01

Daunorubicin toxicity is increased by P2X7A and reduced by P2X7B expression

In an effort to understand the different roles played by P2X7A versus P2X7B in response to daunorubicin, we analyzed the effect of the drug on HEK293 cells expressing the two isoforms separately**.** Therefore, we took advantage of HEK293 cells stably expressing either hP2X7A, hP2X7B or the empty vector for the receptors to perform cell viability assays following daunorubicin administration. In the first set of experiments, we counted the numbers of cells following treatment with 200 nM daunorubicin. Interestingly, daunorubicin toxicity was strongly increased in HEK293 P2X7A cells as compared to mock controls, while expression of P2X7B not only did not affect viability but even protected the cells from daunorubicin-dependent death (Figure 8A). These data were also reproducible in a cell viability assay performed with Alamar blue, thus confirming the death favouring role of P2X7A versus the protective role of P2X7B (Figure 8B).

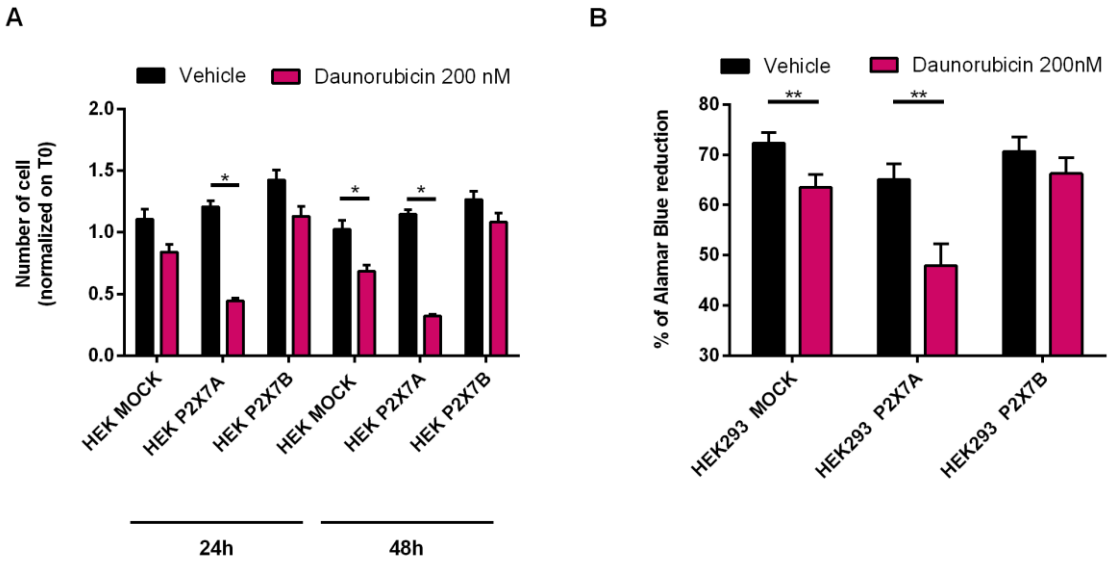

Figure 8 Daunorubicin toxicity is increased by P2X7A and reduced by P2X7B expression. HEK MOCK, HEK P2X7A and HEK P2X7B were seeded at a concentration of $2x10^5$ and treated with vehicle (PBS, 100 µL) or Daunorubicin 200 nM for 48 hours. Five fields for each well were acquired by Leica microscope and counted by ImageJ software. (**A**) Number of cells at 24 and 48 hours after treatment normalized on time 0. Cell viability was assessed also by Alamar Blue assay. 20000 cell/100 µl were seeded in 96-well plate and treated with vehicle (PBS, 100 µL) or Daunorubicin 200 nM for 24 hours. Cell absorbance was measured after 4 hours from the addiction of Alamar Blue. (**B)** The panel represents the percentage of emission at $545nm_{Ex}/590nm_{Em}$, corresponding to the reducing power of living cells.**$p<0.01$

ATP facilitates the permeabilization of HL60 cells to daunorubicin

It is well known that extracellular ATP can cause reversible plasma membrane permeabilization to low molecular weight molecules (< 900 Da) through P2X7 pore opening. In 1994 it was demonstrated that stimulation of P2X7 with ATP can facilitate the entry of the daunorubicin analogous doxorubicin into macrophages [139]. Therefore, we tested if ATP can also facilitate the entrance of daunorubicin into HL60 leukemic cells. ATP treatment significantly increased the entrance of daunorubicin into HL60 cells as compared to control cells (figure 9A). This phenomenon was reversible upon P2X7 blockade (figure 9B).

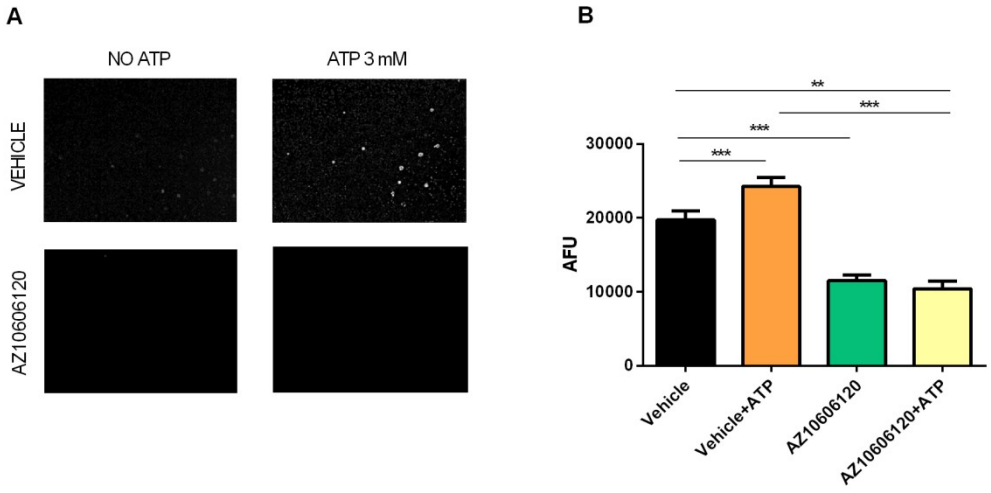

Figure 9 ATP mediates daunorubicin loading in HL60 cells via P2X7 pore opening.

HL60 cells were cultured in saline solution with the addition of daunorubicin 1 µg/ ml , treated or not with AZ10606120 (2 µM) and stimulated or not with ATP 3 mM . (**A**) Images acquired at minute 15 at Leica DMI 4000B microscope. (**B**) Fluorescence data are expressed as arbitrary fluorescent unit (AFU) measured at T15. **p<0.01, ***p<0.001.

P2X7A variant is responsible for increased daunorubicin uptake

In an effort to identify whether P2X7 isoform was responsible for facilitated entry of daunorubicin in leukemic cells, we measured daunorubicin uptake in HEK293 mock, HEK293 hP2X7A and HEK293 hP2X7B cells treated with 3 mM ATP. Figure 10 shows that P2X7A expression significantly increases daunorubicin uptake. While the expression of P2X7B does not affect daunorubicin entry inside the cells.

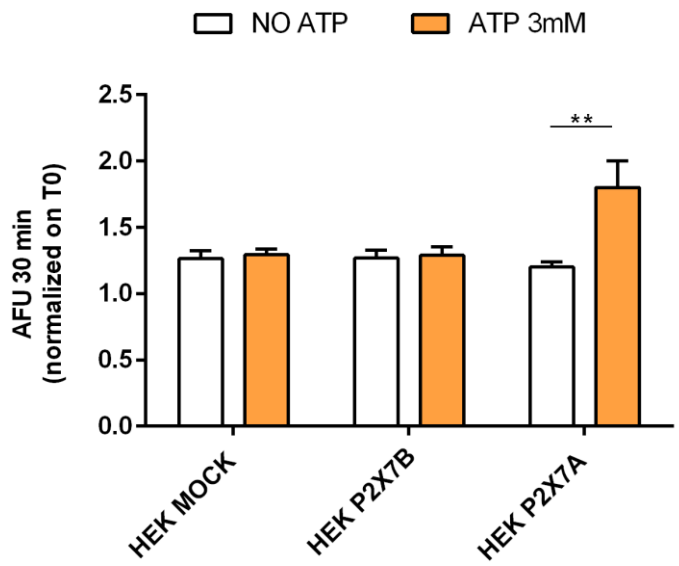

Figure 10 P2X7A facilitates cellular uptake of daunorubicin. HEK MOCK, HEK P2X7A and P2X7B were seeded on a glass coverslip and imaged in standard saline solution with the addition of daunorubicin 1 µg/ml. The uptake of daunorubicin into cells was observed at an inverted microscope measuring fluorescence naturally emitted by daunorubicin. Fluorescence data are expressed as the ratio between the arbitrary fluorescent unit (AFU) measured at T30 and T0 (AFU). **$p<0.01$

DISCUSSION PART I

The tumour microenvironment is rich in components that strongly influence cancer cell survival affecting interaction with immune and stroma cells, extravasation and dissemination. One of the key molecules present in the tumour milieu is ATP, that has a role in the promotion of cancer growth and spreading mainly via its receptor P2X7 [31]. ATP also modulates tumour-associated immune response either via direct activation of inflammatory pathways or indirectly causing immune suppression via generation of its degradation product adenosine by CD39 and CD73 ectonucleotidases activation [140]. Conventional anti-cancer therapy is based on the use of chemotherapeutics that directly kill cancer cells or induce their senescence. However, some chemotherapeutic agents, such as anthracyclines, induce immunogenic cell death (ICD) [11] characterized by the release in the extracellular space of DAMPs including ATP. ATP acts as a potent driver of the immune response against cancer through P2X7 activation on dendritic cells, which are induced to complete maturation to present cancer antigens [11]. Here we analyzed the effect of two different drugs, daunorubicin and ARA-C, which are known respectively to induce or not ICD, on eATP release in an *in vivo* model of leukemia. While daunorubicin and ARA-C treatment had a similar effect on tumour proliferation compared to control (figure 1A), daunorubicin induces the release of more ATP than ARA-C (figure 1B). These data suggest the activation of ICD in tumour bearing mice treated with daunorubicin. Thus, to confirm this hypothesis we analyzed the immune response in all treated mice and we observed that the administration of daunorubicin but not ARA-C promoted a significant increase of IFN-γ, IL-1β, IL-2 and IL-12 (Figure 2). These results show that the increase of eATP in the tumour-bearing mice treated with daunorubicin associates with the activation of a tumour eradicating immune response. To extend the study from the animal model to patient's population we investigated P2X7 expression in an AML cohort. P2X7 modulates important processes during oncogenesis [31] and it can show dual function: upon ATP binding it behaves like a cation-selective channel promoting cell proliferation, while activated by high ATP concentrations causes the opening of large non-selective pore triggering cell death. Among the ten different splice variants, P2X7A and P2X7B are expressed in humans [60]. P2X7A is the full length protein, while P2X7B is the truncated splice variant. Both isoforms are functional ion channels showing growth-promoting activity, while only P2X7A forms the cytotoxic pore. Considering that a wide characterization of P2X7B role in oncogenesis is still missing, we analyzed the differential expression of both P2X7 isoforms A and B in a cohort of patients affected by myelodysplastic syndrome (MDS), a pre-cancerous blood disease that often leading to

AML development, and by acute myeloid leukemia. AML patients were further subdivided according to the diagnostic phases and response to treatment in newly diagnosed untreated subjects (*de novo*), relapsing patients with a return of the pathology after chemotherapy and remitting patients with no evident AML appearance. Both P2X7A and B mRNA levels were strongly increased in firstly diagnosed AML as compared to MDS, supporting the hypothesis that both receptors variants positively correlate with disease progression. Interestingly, AML relapsing patients, which are presented with a return of the pathology after the first therapeutic intervention, were characterized by differential expression of P2X7A and P2X7B as compared to *de novo* patients. Indeed, while P2X7A expression was significantly reduced (figure 4A), P2X7B mRNA significantly increased (figure 4B) suggesting that chemotherapy may cause a decrease in P2X7A expression and on the contrary a positive selection of P2X7B in subjects refractory to treatment. On the contrary, in remitting AML patients both P2X7A and B expression was significantly decreased. These data suggest that individuals expressing high levels of P2X7B could be resistant to chemotherapy and prone to relapse.

Taking into account that all patients experiencing a relapse in AML were treated with daunorubicin and the results obtained from *in vivo* model (Figure 1), we hypothesized that P2X7A expressed by AML cells in presence of high ATP concentration triggers cell death via large pore opening, while P2X7B, that is unable to form the cytotoxic pore, induces leukemic cell proliferation facilitating disease relapse. To confirm our hypothesis, we reproduced patients' data in an *in vivo* model of leukemia using HL60 human cell line expressing both P2X7 isoforms. Tumour-bearing mice were treated with daunorubicin and with a P2X7 antagonist, alone or in co-administration. Both compounds significantly reduced leukemia growth, but their co-administration was more efficacious than the single-drug treatment. Daunorubicin effect on P2X7 isoforms expression was similar to the patient's data as P2X7B expression was significantly increased by daunorubicin while P2X7A showed a tendency to decrease. Interestingly, the co-administration of daunorubicin with P2X7 antagonist normalized both P2X7A and B levels suggesting that P2X7 antagonist may counteract the effect of daunorubicin on cells predominantly expressing P2X7B. To analyze the differential effect of P2X7A and P2X7B in response to daunorubicin, we took advantage of HEK293 cells transfected with the two isoforms separately. Interestingly, daunorubicin toxicity was strongly increased in HEK P2X7A as compared to controls, while the expression of P2X7B protected the cells from daunorubicin-dependent death. Thus, we wondered whether P2X7A-mediated pore opening could facilitate the entrance of daunorubicin into tumour cells, as it was

demonstrated in macrophages for its analogous doxorubicin [139]. Indeed, this proved to be the case as in HL60 cells, that express both isoforms, P2X7 blockade decreases daunorubicin uptake. This phenomenon was solely dependent on P2X7A that is the only isoform significantly increases daunorubicin uptake (Figure 10).

The relapse of AML after chemotherapy is the main cause of patients' death and efforts to improve their survival is the main goal for onco-hematologists. Our study suggests that P2X7 could be a good target in AML therapy. We can speculate that a combined therapy in which daunorubicin is administered first, to eliminate leukemic cells expressing P2X7A, while P2X7 antagonist is administered in a second phase to block P2X7B expressed by blasts resistant to the cytotoxic effect of daunorubicin will be a suitable approach in AML treatment.

RESULTS CHAPTER II

Role of P2X7 receptor in extracellular ATP modulation, tumour progression and cell vesicle release in melanoma experimental models.

P2X7 antagonism reduces primary melanoma growth in mice.

We reproduced an *in vivo* model of melanoma by subcutaneously injecting murine B16 cells in C57BL/6 syngeneic mice. In an effort to elucidate the role of P2X7 in tumour growth, P2X7 antagonist A740003 (20 µM) or placebo (PBS with 0.005% DMSO, 100µl) were intra-peritoneum injected every two days after day 5 corresponding to first tumour mass detection. A740003 administration significantly reduced tumour growth as compared to placebo.

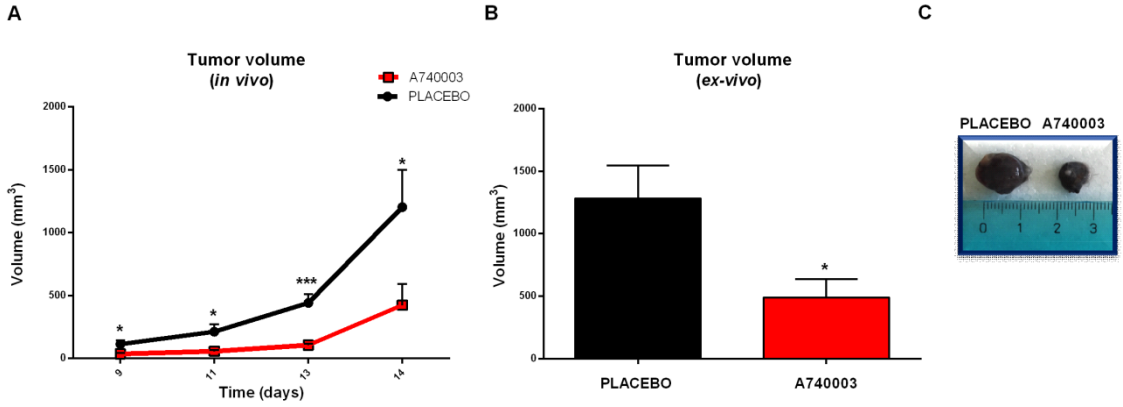

Figure 1 P2X7 antagonist A740003 significantly reduces tumour growth. (**A**) Tumour volume was assessed every other day from day 5. (**B**) *Ex vivo* tumour volume. (**C**) Representative pictures of tumours from mice treated with placebo (PBS) and A740003 (20 µM). Data are shown as the mean ± SEM of 8 mice per condition. **p< 0.01.

P2X7 blockade down modulates CD39 and CD73 expression

To correlate P2X7 with the adenosine generating pathway that is involved in ATP degradation and tumour immune suppression, we analysed the expression of ectonucleotidases in tumour infiltrating immune cells. This pathway includes CD39, which is responsible for the conversion of ATP into ADP and AMP, and CD73, which hydrolyzes AMP into adenosine. As shown in Figure 2, P2X7 antagonism decreases CD39 and CD73 ectonucleotidases expression on dendritic cells (cDC) and effector $CD4^+$ T cells (Teff) suggesting that P2X7 blockade can reduce ATP degradation into adenosine and cause the enrichment of ATP in the tumour microenvironment.

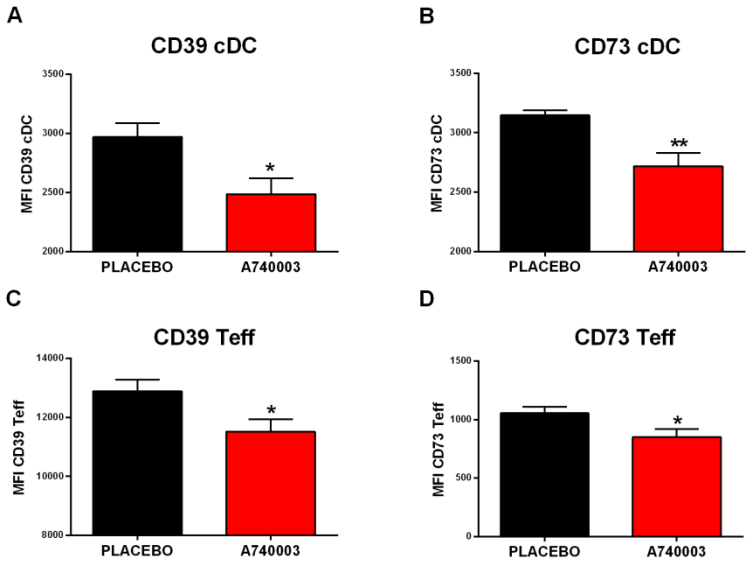

Figure 2 P2X7 antagonism decreases ectonucleotidases expression on effector T cell and dendritic cells. Flow cytometric analysis of tumour masses from C57BL/6 mice treated with placebo (PBS with 0.005% DMSO, 100µL) or A740003 (20 µM). MFI of CD39 (**A**) and CD73 (**B**) on cCD; MFI of CD39 (**C**) and CD73 (**D**) on Teff. Data are shown as the mean ± SEM of 8 mice per condition. *p<0.05, **p<0.01.

P2X7 pharmacological blockade has no effect on tumour microenvironment ATP

Based on ectonucleotidases data, we further investigated the effect of P2X7 blockade on ATP release from melanoma-bearing mice following of A740003 administration. This P2X7 antagonist while significantly reducing tumour growth as shown in Figure 1, did not affected ATP concentration in the tumour microenvironment as compared to the control (placebo) Figure 3.

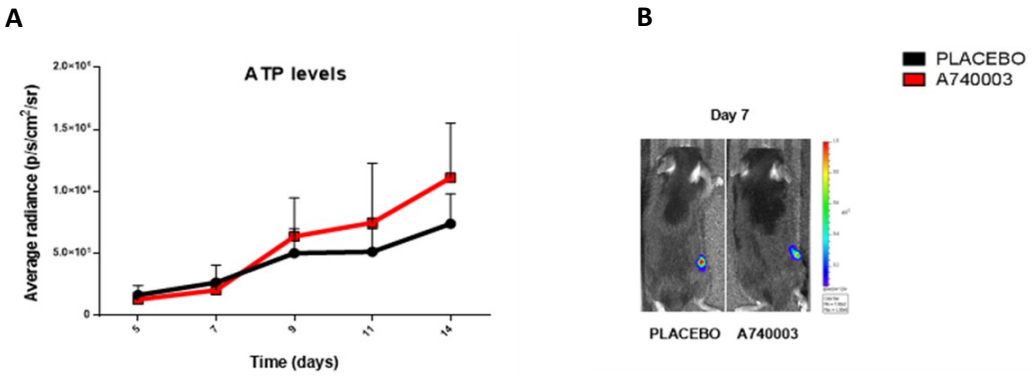

Figure 3 P2X7 blockade did not affect ATP levels in the tumour microenvironment C57BL/6 mice were inoculated into the right hind flank with B16 pmeLUC. (**A**) ATP levels in the tumour microenvironment estimated by pmeLUC luminescence emission expressed as average radiance (p/s/cm^2/sr). (**B**) Representative pictures of pmeLUC luminescence emission in C57BL/6 at day 7. Data are shown as the mean ± SEM of 8 mice per condition.

P2X7 blockade causes an increase of ATP released from cancer cells while reducing eATP coming from immune cells

To better understand data shown in Figure 3, we measured ATP release from peritoneal macrophages isolated from C57BL/6 mice and B16 cells alone or in co-culture. P2X7 antagonism caused a significant rise in ATP released by B16 cells compared vehicle, while decreasing ATP released by macrophages (Figure 4A). Interestingly, the co-culture of macrophages with B16 cells promoted an increase in eATP. However, A740003-stimulated increase in ATP release was lost in B16 cells and macrophages co-culture. Taken together these data suggest that the overall content of ATP in the tumour microenvironment remains unaltered (Figure 3) due to the opposite effect of P2X7 antagonism on tumour versus immune cells.

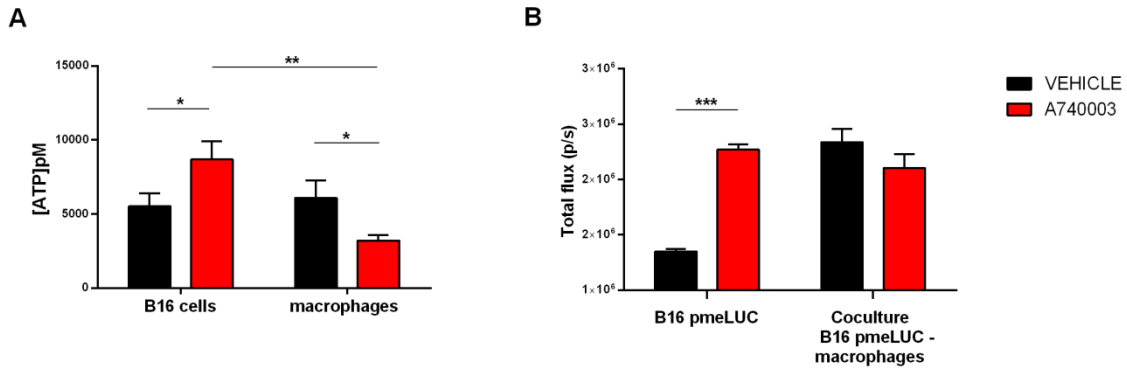

Figure 4 P2X7 antagonism in the co-culture of tumour cells and macrophages results in unaltered ATP levels. (A) Extracellular ATP levels in B16 pmeLUC cells and peritoneal macrophages derived from C57BL/6 mice treated with A740003 20 μM. (**B**) Extracellular ATP levels in B16 pmeLUC cells alone or in co-culture with macrophages treated with vehicle (PBS + 0.05% DMSO, 100μl) or A740003 20 μM.

Human metastatic melanoma shows increased P2X7 expression

The results obtained in our murine model of melanoma suggest that P2X7 antagonism has good potential as an anticancer treatment in the primary tumour. However, it is well known that P2X7 participates in tumour cell dissemination by favouring angiogenesis, causing extracellular matrix remodelling and preparing the pre-metastatic niche. At the moment a direct association between P2X7 activity and melanoma dissemination is still missing. Therefore, we investigated the role of the P2X7 receptor in melanoma dissemination in a human metastatic melanoma model focusing on vesicles release, a phenomenon recognized as a crucial for cancer spreading and metastasis formation. To verify if there is an association between P2X7 expression and melanoma aggressiveness we performed immunohistochemical analysis on human melanoma specimens. A total of 59 tumour samples were tested among which 14 were from metastatic melanoma. All samples stained positive for P2X7 (Figure 5A and 5B), however, 85 % of those obtained from patients with metastatic melanoma showed stronger positivity for P2X7 than 57% found in non-metastatic cases (Figure 5C).

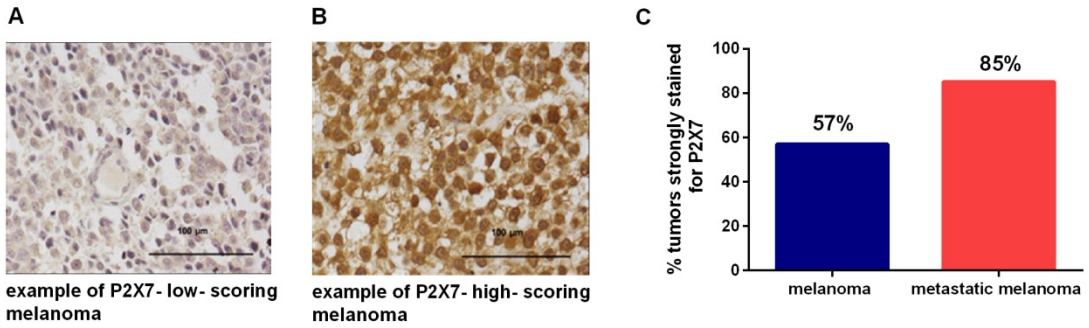

Figure 5 Human metastatic melanoma shows increased P2X7 expression. Immunohistochemistry with an antibody directed against P2X7 cytoplasmic tail was performed on Super Bio chips tissue slides covering 59 melanoma including 14 metastatic specimens. Representative images of immunohistochemistry performed on non-metastatic (**A**) and metastatic (**B**) melanomas. (**C**) Percentage of metastatic and non-metastatic melanoma samples with strong positivity for P2X7.

Correlation of P2X7A and P2X7B expression with melanoma progression and metastatic spread

To substantiate data shown in Figure 5, we investigated P2X7A and P2X7B expression of a 77 cDNA array obtained from melanoma patients subdivided according to the stage and metastasis location in stage III, stage IV with skin metastasis, stage IV with lung metastasis and stage IV with metastases in other distant organs including liver and brain, by Real-Time PCR. We observed that the expression of both isoforms A and B increases with the spreading ability of melanoma cells. Both P2X7A and P2X7B are significantly overexpressed in stage IV melanoma with metastasis at lungs and in other distant organs.

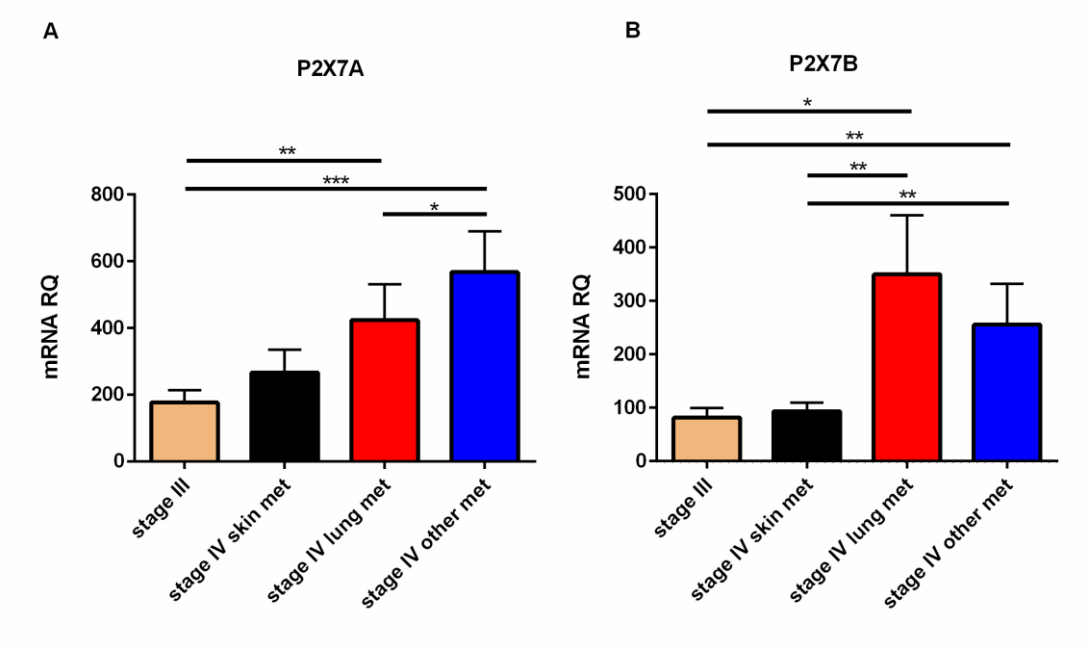

Figure 6 Both P2X7A and P2X7B are highly expressed in the IV stage melanomas with distant metastasis. (**A**) P2X7A and (**B**) P2X7B mRNAs expression was evaluated by Real-Time PCR in 77 cDNAs from melanoma patients subdivided in stage III (n=27), stage IV with skin metastasis (n=15), stage IV with lung metastasis (n=10) and stage IV with metastases in other distant organs (n=14). *p<0.05, **p<0.01, ***p<0.001

Characterization of functional P2X7 receptor in human melanoma cell lines

In an effort to identify an human melanoma cell line expressing both P2X7A and P2X7B and suitable for following experiments we investigated the presence of a functional P2X7 receptor in: A-2058, GR-M, A-375, Sk-Mel-28 and Ma-Mel-19 cells. P2X7 activity was evaluated measuring the change of intracellular calcium concentration ($[Ca^{2+}]_i$) following P2X7 stimulation with its agonist BzATP (300 μM). Sk-Mel-28 and Ma-Mel-19 cell lines

express a functional P2X7 receptor as evidenced by the increase of calcium concentration upon P2X7 stimulation with BzATP (Figure 7A-7B), while A-2058, GR-M and A-375 show no changes in cytoplasmic calcium concentration (Figure 7C-7D-7E).

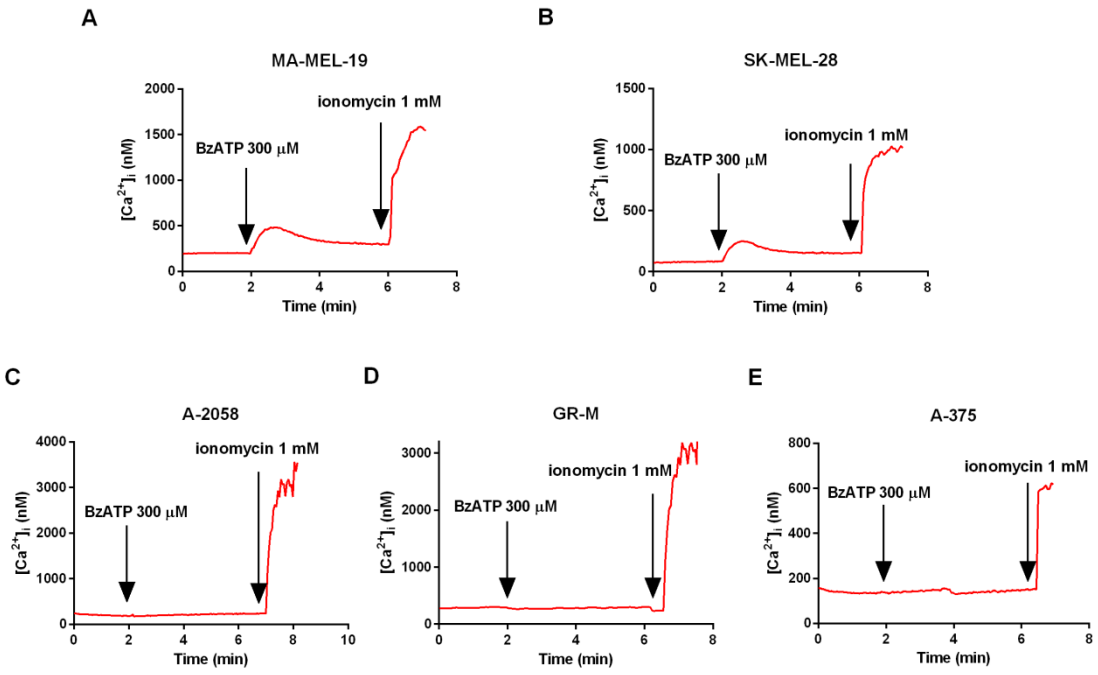

Figure 7 Ma-Mel-19 and Sk-Mel-28 cell lines express a functional P2X7 receptor. P2X7 activity assay in human melanoma cell lines. Cells were incubated with standard saline solution in the presence of Ca^{2+} and fluorescent dye *FURA-2/AM* and P2X7 receptor activity was evaluated measuring variations in $[Ca^{2+}]i$ following stimulation with the agonist BzATP (300 µM). 1 mM ionomycin was added to verify FURA-2/AM loading. P2X7 activity of (**A**) Ma-Mel-19, (**B**) Sk-Mel-28, (**C**) A-2058, (**D**) GR-M and (**E**) A-375 cells.

To confirm that BzATP specifically activates the P2X7 receptor in the tested cell lines we also performed *FURA-2/AM* uptake experiments in the presence of two different P2X7 antagonists A740003 (20 µM) and AZ10606120 (2 µM). As shown in Figure 8 the effect of 300 µM BzATP was completely blocked by pre-incubation with both P2X7 receptor antagonists.

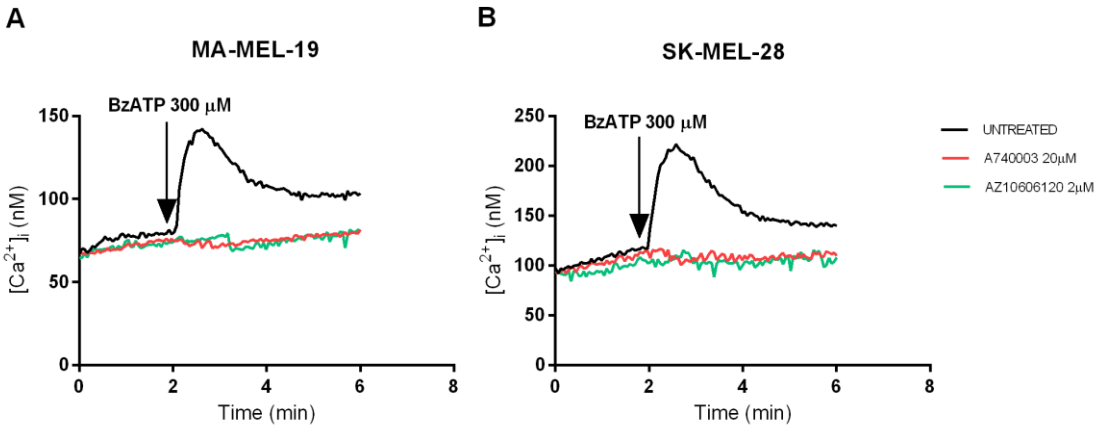

Figure 8 A740003 and AZ10606120 inhibit P2X7 receptor activity in Ma-Mel-19 and Sk-Mel-28. (**A-B**) Sk-Mel-28 and Ma-Mel-19 cells were incubated with 20 μM A740003 and 2 μM AZ10606120, in standard saline solution with Ca^{2+} and fluorescent dye *FURA-2/AM*. P2X7 receptor activity was evaluated measuring variations in $[Ca^{2+}]_i$ following stimulation with the agonist BzATP (300 μM). The P2X7 receptor antagonists A740003 and AZ10606120 completely oblitered the effect of BzATP in both (**A**) Ma-Mel-19 and (**B**) Sk-Mel-28 cell lines.

We then investigated the expression of P2X7A and P2X7B in Sk-Mel-28 and Ma-Mel-19 cells by Real-Time PCR showing that both cell lines express P2X7A and P2X7B mRNA.

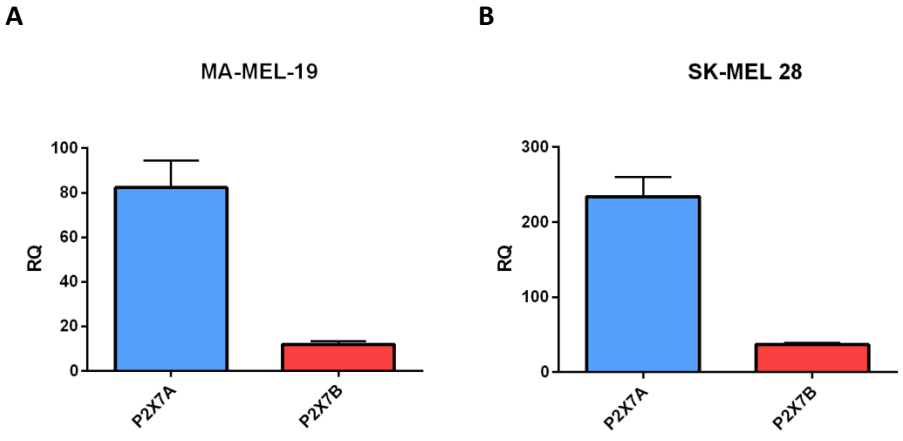

Figure 9 Both P2X7A and P2X7B mRNAs are expressed by Ma-Mel-19 and Sk-Mel-28. Analysis of mRNA expression of P2X7 isoforms A and B in (**A**) Ma-Mel-19 and (**B**) Sk-Mel-28 human melanoma cell lines by Real-Time PCR.

P2X7 antagonists reduce Sk-Mel-28 and Ma-Mel-19 cells proliferation, anchorage-independent growth ability and migration

The following *in vitro* experiments were performed to evaluate the effects of P2X7 antagonists on proliferation, transformation ability and migration of Sk-Mel-28 and Ma-Mel-19 and human melanoma cell lines. Figures 10 shows the anti-proliferative activity of P2X7 antagonists A740003 and AZ10606120 on Sk-Mel-28 and Ma-Mel-19 cells.

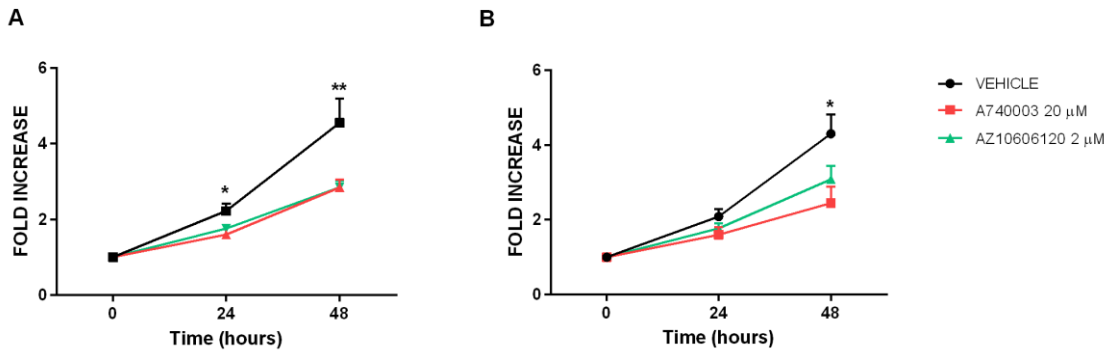

Figure 10 A740003 and AZ10606120 reduce Sk-Mel-28 and Ma-Mel-19 proliferation. Cells were treated with the vehicle (PBS), A740003 (20 µM) and AZ10606120 (2 µM). Images of cells were taken at time 0 and after 24 and 48 hours from the treatment. Sk-Mel-28 (**A**) and Ma-Mel-19 (**B**) cells were counted with the software ImageJ and data are presented as fold increase of time 0. Data are shown as the mean ± SEM of 3 experiments. *p<0.05, **p<0.01

A soft agar colony formation assay allow us to evaluate the capacity of P2X7 antagonists to reduce cellular transformation in *vitro*. Figure 11 show the tumour-suppressive effects of the two different P2X7 antagonists, A740003 and AZ10606120, causing inhibition of colony formation. Cells were plated onto soft agar plates and allowed to form colonies for twenty days. The number of colonies formed by cells treated with P2X7 antagonists is strikingly reduced as compared to control cells (Figure 11).

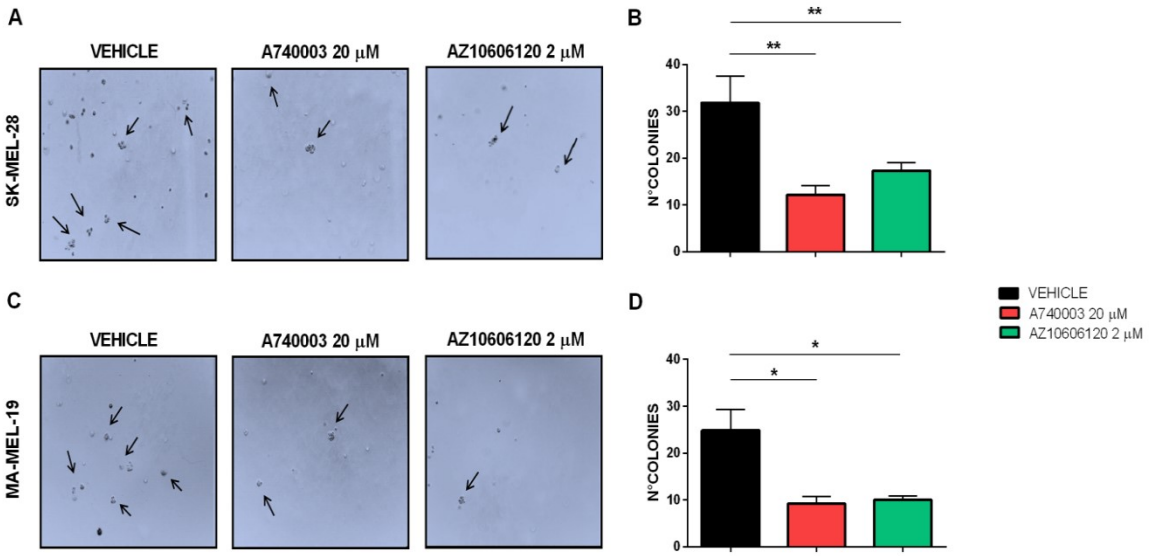

Figure 11 Both P2X7 antagonists reduce the capacity of cells to form colonies in soft agar plates. (**A** and **C**)) Representative pictures for each treatment showing cell colonies. (**B** and **D**) Number of colonies formed. Data are shown as the mean ± SEM of 3 experiments. Black arrows indicate colonies, **p<0.01

Finally, we performed a scratch assay to measure the effect of P2X7 antagonists on cell migration *in vitro*. We measured scratch areas after 24 and 48 hours of incubation with the two P2X7 antagonists. A740003 and AZ10606120 significantly decreased the scratch closing rate at 24 hours as compared to the control.

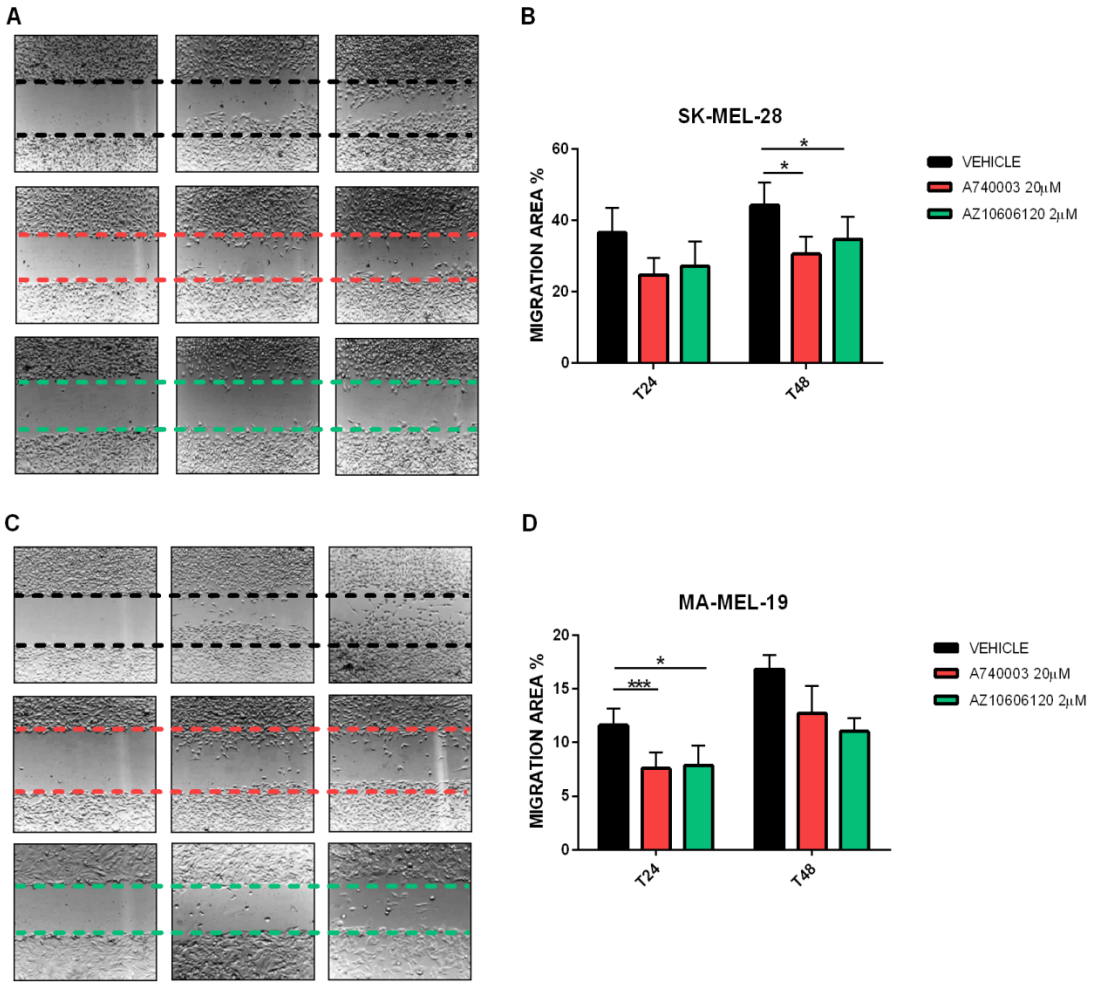

Figure 12 P2X7 antagonists reduce Sk-Mel-28 and Ma-Mel-19 migration ability. Representative images of scratches taken at time 0, 24 and 48 of Sk-Mel-28 (**A**) and Ma-Mel-19 (**C**). Cells were plated onto a 6-well plate and when they have grown to a confluence a scratch was made with a sterile pipette tip. Treatment with A740003 (20 µM) and AZ10606120 (2 µM) P2X7 antagonists reduced the scratch closing rate. (**B** and **D**) Quantitative analysis expressed as the percentage of the migration area. Data are shown as the mean ± SEM of 3 experiments *p<0.05

Systemic administration of P2X7 antagonist A740003 reduces tumour dissemination in murine melanoma model.

We performed an *in vivo* experiment using Sk-Mel-28 cells to investigate the role played by P2X7 in melanoma cell dissemination and metastasis formation. Sk-Mel-28 cells, transfected with an intracellular luciferase (Luc2) were injected into the tail vein of athymic nude mice divided into two groups, that were treated with a peritoneal injection of placebo or with P2X7 antagonist A740003 (20 µM) every 72 hours for 45 days. Cell dissemination was followed by measuring luciferase photon emission thanks to a luminometer for small animals and mice were sacrificed at day 45. The kinetic analysis of photon emission (Figure 16A) shows that P2X7 antagonism slows down melanoma spreading, in particular we found a significant difference in photon emission at day 33 from inoculum (Figure 16B).

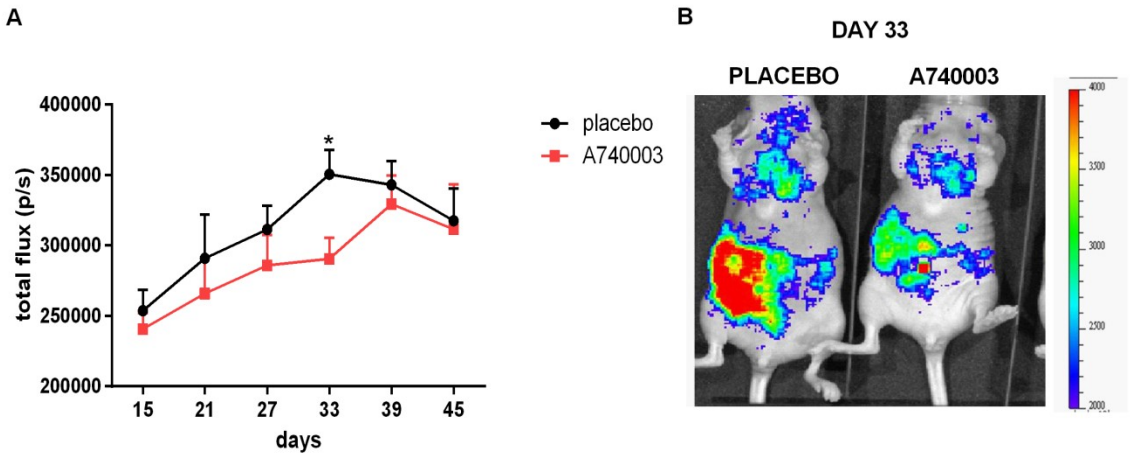

Figure 16 A740003 reduces Sk-Mel-28 melanoma cell spread. (**A**) Photons emission measured every six days in mice treated with placebo (PBS, 100 µL) or with A740003 (20 µM). Luminescence emission is presented as total flux (p/s). Data are shown as the mean ± SEM of 8 mice per condition (**B**) Image of Luc2 luminescence emission captured thanks to a luminometer for small animals in placebo and A740003 treated mice on day 33. *p<0.05

Human melanoma cells release extracellular vesicles upon stimulation with ATP

Extracellular vesicles released by tumour cells contribute to different biological processes such as tumour growth, angiogenesis, cell dissemination and formation of the pre-metastatic niche at a distant site from the primary tumour. Activation of P2X7 was already associated with vesicles release in immune cells, but at the moment a direct association between P2X7 activity and vesicles released from tumour cells is missing. Single-cell optical (Figure 17) and electron microscopy (Figure 18) experiments allowed us to estimate that both Ma-Mel-19 and Sk-Mel-28 cell line release vesicles in the size range of 100-800 nm and that P2X7 stimulation increases their release.

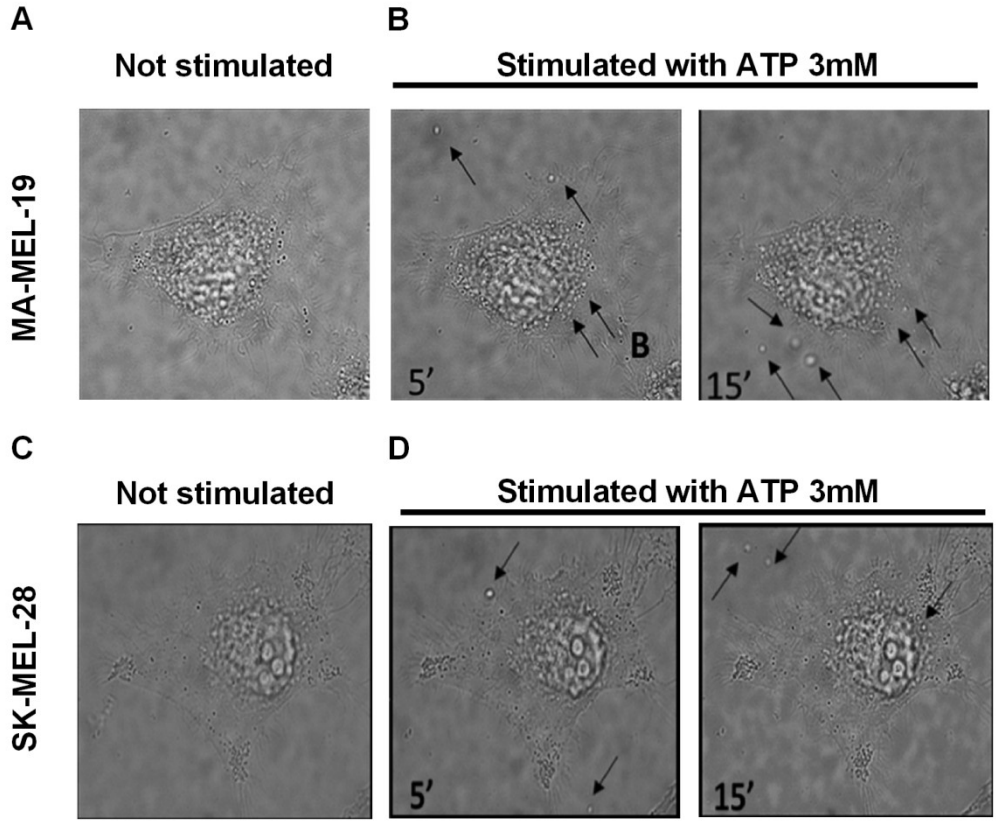

Figure 17 ATP triggers vesicles shedding from Ma-Mel-19 and Sk-Mel-28 cells. Cells were seeded on glass coverslips in standard saline solution and left without treatment or treated with ATP 3 mM. Images were acquired at five-seconds intervals using the MetaMorph software with the Nikon Eclipse T-300 microscope. (**A**) and (**C**) representative images of not stimulated cells. (**B**) and (**D**) representative images of vesicles released from melanoma cells captured 5 and 15 minutes after stimulation. Black arrows indicate released vesicles.

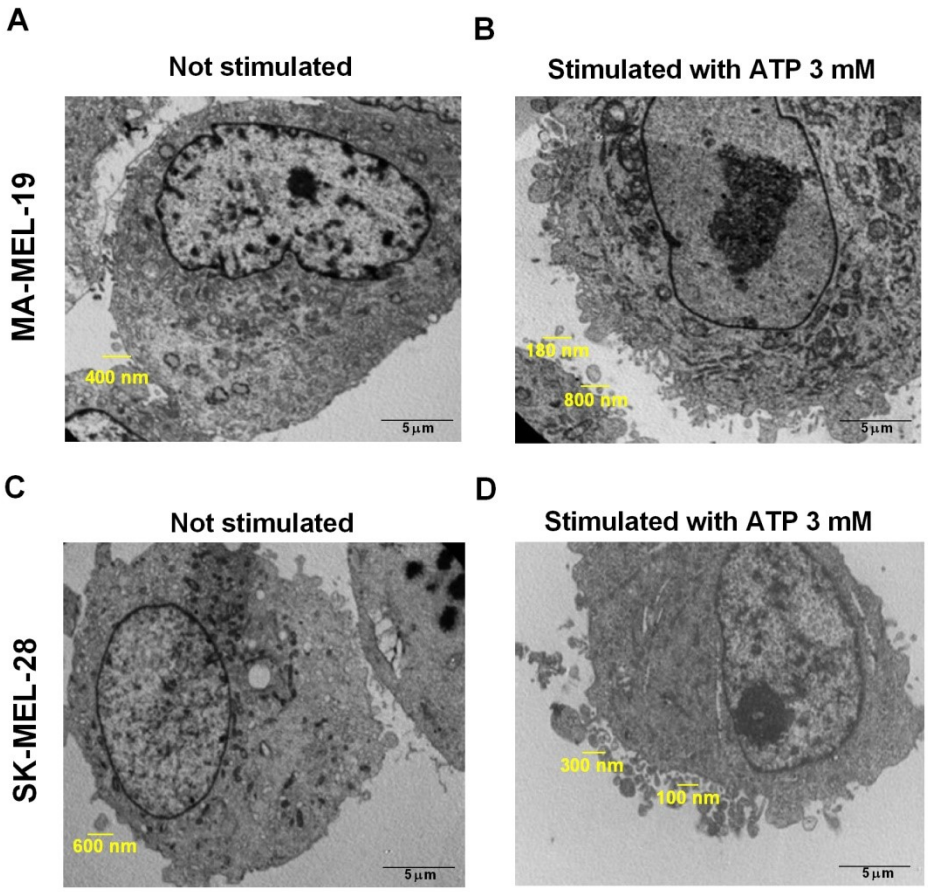

Figure 18 Electron microscopy analysis of Ma-Mel-19 and Sk-Mel-28 cells stimulated with ATP. Cells incubated in saline solution at 37 °C were left untreated (**A** and **C**) or stimulated with 3 mM ATP (**B** and **D**) for 10 minutes. Cells were then detached from flasks, fixed with glutaraldehyde and processed for electron microscopy. Representative images of not stimulated cells (**A-C**) and cells stimulated with ATP (**B-D**). Morphometric analysis indicated vesicle size in the range between 100 nm and 800 nm.

ATP stimulation affects vesicles release from melanoma cells

The heterogeneous size of vesicles estimated by electron microscopy analysis (Figure 18) led us to hypothesize P2X7 dependent release of different types of vesicles from melanoma cells. Therefore, we decided to separate small and large vesicles using the ultracentrifugation protocol for microvesicles and exosomes isolation. The larger vesicles were isolated with ultracentrifugation at 18.000 x g for 40 minutes, while the smaller vesicles with ultracentrifugation at 100.000 x g for four hours. We then estimated vesicle dimensions and concentration with the Nanoparticle tracking analysis (NTA) using a Nanosight instrument. The analysis was performed comparing the parameters of vesicles released from untreated and ATP stimulated cells. Results show that ATP treatment of Ma-Mel-19 cells induces a significant decrease of large vesicles and a significant increase of the size of both vesicle fractions as compared to the control (Figure 19B, 19D), while Sk-Mel-28 treated with ATP release a significantly higher number as compared to the control (Figure 19F).

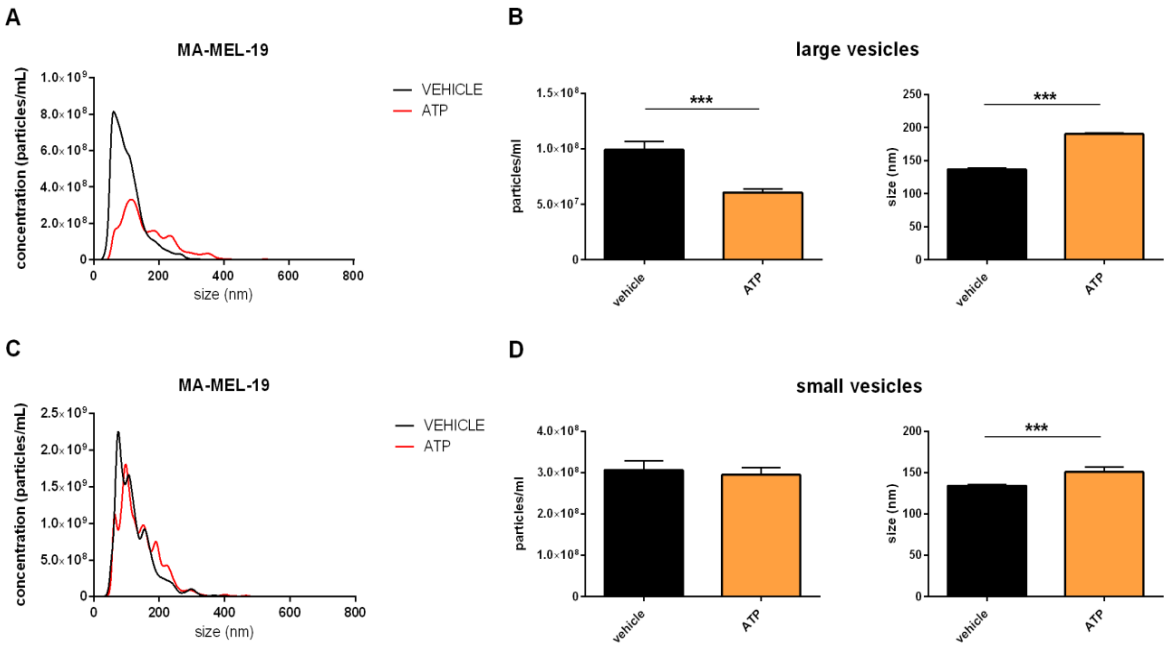

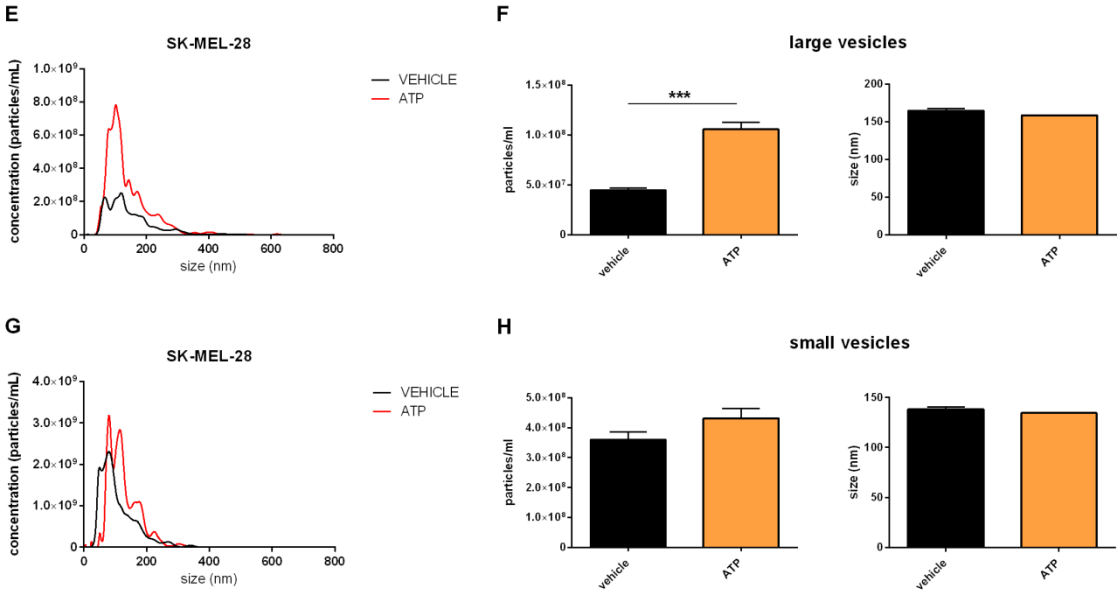

Figure 19 ATP stimulation affects vesicles release from melanoma cells. Thanks to Nanosight vesicles are visualized by light scattering using the NTA software that tracks the Brownian motion of individual vesicles from video images and calculates their size and total concentration. (**A-C-E-G**) Representative graphs of size distribution and concentration obtained from the analysis of five different videos. Comparison of concentration and size between large (**B**) and small (**D**) vesicles released from control and ATP treated Ma-Mel-19 cells. Comparison of concentration and size between large (**F**) and small (**H**) vesicles released from control and ATP treated Sk-Mel-28 cells. ***p<0.01

ATP stimulation alters microRNA content of both small and large vesicles released from melanoma cells.

Analysis by small RNA sequencing of the miRNA content of small and large vesicles obtained from both Sk-Mel-28 and Ma-Mel-19 cells, before and after ATP stimulation, shows a different global miRNA expression profile. On a total of 2553 microRNAs analyzed, ATP stimulation of the receptor caused differential expression of 251 miRNAs in Sk-Mel-28 small vesicles, of 191 miRNAs in Sk-Mel-28 large vesicles, of 91 miRNAs in Ma-Mel-19 small vesicles and of 206 miRNAs in Ma-Mel-19 large vesicles (Figure 20). The most up-regulated miRNAs by ATP stimulation were: miR-495-3p (p = 1.69E-06), miR-4755-3p (p= 1.57E-05), miR-4638-5p (p = 2.17E-05) and miR-6730-3p (p= 2.30E-05) found in small vesicles released from both melanoma cell lines. Future experiments are needed to validate these over-expression miRNAs through Real-Time PCR and to assess their effects on cancer cell proliferation, dissemination and metastasis formation.

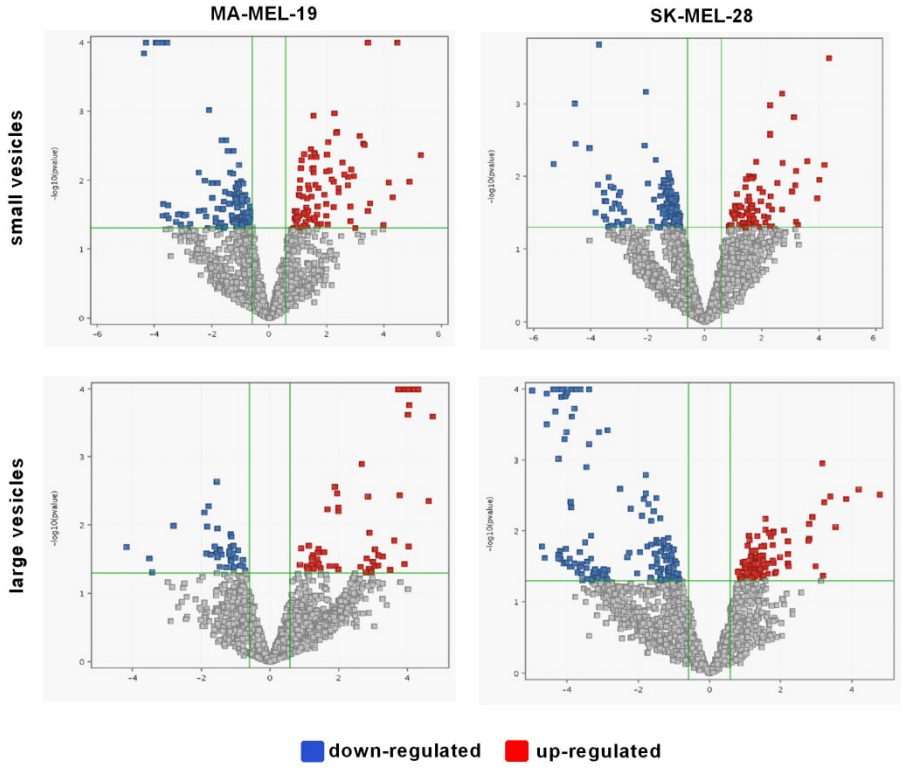

Figure 20 Volcano plots showing miRNAs differentially expressed in small and large vesicles upon P2X7 stimulation. The analysis of a total of 2553 microRNAs was performed by using sample triplicates, with a 1.5 fold change filter and moderated t-test for group comparison. Raw data were processed using the Qiagen Gene Globe Data Analysis Center to obtain quantification.

DISCUSSION PART II

The P2X7 for ATP is a promising therapeutic target in oncology due to the efficacy of P2X7 antagonists to reduce tumour growth [54, 55]. However, P2X7 is expressed also by immune cells that are present in the tumour microenvironment and its activation is associated with anti-tumoural immune response. ATP can also favor an immune suppression as it is the main substrate for the production of adenosine via CD39 and CD73 ectonucleotidases mediated hydrolysis. In an effort to identify *in vivo* the effect of the selective tumour-P2X7 blockade, we investigated the impact of P2X7 antagonism on tumour growth and ATP release in a melanoma model. We demonstrated that the administration of the P2X7 antagonist significantly reduces tumour growth but doesn't affect ATP levels in the tumour microenvironment. Thus, we analyzed the ectonucleotidases expression on tumour-infiltrating immune cells that allowed us to correlate P2X7 with the adenosine-generating pathway. Both CD39 and CD73 ectonucleotidases are down modulated, suggesting that the P2X7 blockade reduces ATP degradation into adenosine. To identify the source of ATP in the tumour microenvironment, we measured *in vitro* ATP release from immune and cancer cells alone or in co-culture. P2X7 antagonism induces an increase of ATP released from melanoma cells, while reduces ATP levels in immune cells. Interestingly, the co-culture of cancer with immune cells results in a significant increase in peri-cellular ATP. However, the P2X7 blockade-stimulated increase in ATP release was lost in cancer and immune cells co-culture, suggesting that P2X7 antagonist, on the one hand, increases ATP release from tumour cells, but on the other decreases it from immune cells, thus leaving unaltered the overall content of ATP in the tumour microenvironment. The tumour growth inhibition observed in our *in vivo* melanoma model supports the hypothesis that the administration of P2X7 antagonists may be a viable therapy for melanoma. However, the great challenge in the treatment of melanoma is the metastatic forms that are resistant to current therapeutic approaches. Despite it is known that P2X7 is involved in angiogenesis, extracellular matrix degradation, cell migration and colonization of distant tissue, a direct association between P2X7 activity and melanoma dissemination is still missing. The analysis of mRNA from human melanoma samples allowed us to correlate the high expression of P2X7 with melanoma with metastases at distant sites such as the lungs or the liver. These data were further confirmed by immunohistochemical analysis of specimens from metastatic and non-metastatic melanoma patients in which metastatic samples showed strong positivity for P2X7. Metastasis formation requires cancer cell migration, local invasion, pre-conditioning and colonization of secondary sites. We analyzed the P2X7 role in melanoma

invasiveness and we verified the effects of its antagonists in different *in vitro* and *in vivo* melanoma experimental models. We performed the experiments using two human metastatic melanoma cell lines expressing P2X7: Sk-Mel-28 and Ma-Mel-19. P2X7 antagonists proved efficacious in reducing cell proliferation, wound closure by scratch test and colony growth on soft agar. We also demonstrated a reduction of melanoma dissemination and metastasis formation, upon systemic P2X7 pharmacological blockade in nude mice injected with Sk-Mel-28 cells. Aiming at identifying the mechanisms activated by P2X7 in metastatic melanoma, we studied the release of vesicles from Sk-Mel-28 and Ma-Mel-19 cells following P2X7 stimulation with the agonist ATP. It is well known that vesicles released from cancer cells are involved in intercellular communication, tumour growth promotion and metastatic evolution. It was already demonstrated that activation of P2X7 mediated the release of microvesicles from immune cells but there is no in-depth information about this phenomenon in cancer cells. Single-cell optical and electron microscopy experiments allowed us to estimate that both cell lines release vesicles in the size range of 100–800 nm and that P2X7 stimulation increases their release. These data were also confirmed by estimating vesicle concentration and dimensions with the Nanosight platform, following the separation of small and large vesicles by ultracentrifugation at different speeds. P2X7 stimulation caused a general increase in vesicle concentration and dimensions. Analysis by small RNA sequencing of the miRNA content of large and small vesicles obtained from both Sk-Mel-28 and Ma-Mel-19 cells, before and after P2X7 stimulation, showed a different global miRNA expression profile. On a total of 2553 microRNAs analyzed, ATP stimulation of the receptor caused differential expression of 251 miRNAs in Sk-Mel-28 small vesicles, of 191 miRNAs in Sk-Mel-28 large vesicles, of 91 miRNAs in Ma-Mel-19 small vesicles and of 206 miRNAs in Ma-Mel-19 large vesicles. Among these miRNAs differentially expressed after P2X7 stimulation, four miRNAs are the most up-regulated in small vesicles of both cell lines: miR-495-3p, miR-4755-3p, miR-4638-5p and miR-6730-3p. We plan to validate miRNAs upregulation by Real-Time PCR analysis and, due to the limited literature actually available on the function of these miRNAs, further asses their effects on cancer cell proliferation, dissemination, and metastasis formation. Despite the introduction of immune therapy has increased substantially metastatic melanoma patient's life expectancy, these therapies are generally expensive and limited to a discrete population or associated with immune-related adverse events in patients. Results obtained in our study confirm the role of P2X7 in melanoma invasiveness may be due to vesicles release, and point to as P2X7 a potential pharmacological target for advanced melanoma treatment.

ACKNOWLEDGMENTS

For this work I would like to thank:

My tutor Prof. Elena Adinolfi and my colleagues Dr. Elena De Marchi and Dr. Elisa Orioli.

Prof. Francesco Di Virgilio and his research group.

Dr. Antonio Curti, Dr. Valentina Salvestrini and Dr. Mariangela Lecciso from Institute of Hematology L. and A. Seràgnoli, S.Orsola - Malpighi Hospital of Bologna that provide us with leukemia clinical samples.

Prof. Manuela Ferracin from University of Bologna who substantially helped us to design the experimental model about miRNA and performed the analysis of microRNA expression.

Dr. Anna Tesei and Dr. Michele Zanoni from IRST of Meldola who performed Nanoparticle Tracking Analysis with Nanosight platform.

Prof. Massimo Negrini, Dr. Cristian Bassi and Dr. Lucilla D'Abundo from University of Ferrara who performed NGS sequencing.

BIBLIOGRAPHY

1. Bonora, M., et al., *ATP synthesis and storage.* Purinergic Signal, 2012. **8**(3): p. 343-57.
2. Burnstock, G., et al., *Evidence that adenosine triphosphate or a related nucleotide is the transmitter substance released by non-adrenergic inhibitory nerves in the gut. 1970.* Br J Pharmacol, 1997. **120**(4 Suppl): p. 337-57; discussion 334-6.
3. Burnstock, G., *Purinergic nerves.* Pharmacol Rev, 1972. **24**(3): p. 509-81.
4. Pellegatti, P., et al., *Increased level of extracellular ATP at tumour sites: in vivo imaging with plasma membrane luciferase.* PLoS One, 2008. **3**(7): p. e2599.
5. Hazama, A., et al., *Swelling-activated, cystic fibrosis transmembrane conductance regulator-augmented ATP release and Cl- conductances in murine C127 cells.* J Physiol, 2000. **523 Pt 1**: p. 1-11.
6. Forrester, T. and C.A. Williams, *Release of adenosine triphosphate from isolated adult heart cells in response to hypoxia.* J Physiol, 1977. **268**(2): p. 371-90.
7. Martins, I., et al., *Chemotherapy induces ATP release from tumour cells.* Cell Cycle, 2009. **8**(22): p. 3723-8.
8. Lazarowski, E.R., *Vesicular and conductive mechanisms of nucleotide release.* Purinergic Signal, 2012. **8**(3): p. 359-73.
9. Di Virgilio, F., *Purines, purinergic receptors, and cancer.* Cancer Res, 2012. **72**(21): p. 5441-7.
10. Stagg, J. and M.J. Smyth, *Extracellular adenosine triphosphate and adenosine in cancer.* Oncogene, 2010. **29**(39): p. 5346-58.
11. Garg, A.D., et al., *Immunogenic cell death, DAMPs and anticancer therapeutics: an emerging amalgamation.* Biochim Biophys Acta, 2010. **1805**(1): p. 53-71.
12. Garg, A.D., et al., *A novel pathway combining calreticulin exposure and ATP secretion in immunogenic cancer cell death.* EMBO J, 2012. **31**(5): p. 1062-79.
13. Zitvogel, L., et al., *Inflammasomes in carcinogenesis and anticancer immune responses.* Nat Immunol, 2012. **13**(4): p. 343-51.
14. Ghiringhelli, F., et al., *Activation of the NLRP3 inflammasome in dendritic cells induces IL-1beta-dependent adaptive immunity against tumours.* Nat Med, 2009. **15**(10): p. 1170-8.
15. Martins, I., et al., *Molecular mechanisms of ATP secretion during immunogenic cell death.* Cell Death Differ, 2014. **21**(1): p. 79-91.

16. Ohta, A. and M. Sitkovsky, *Role of G-protein-coupled adenosine receptors in downregulation of inflammation and protection from tissue damage.* Nature, 2001. **414**(6866): p. 916-20.
17. Michaud, M., et al., *Autophagy-dependent anticancer immune responses induced by chemotherapeutic agents in mice.* Science, 2011. **334**(6062): p. 1573-7.
18. Beigi, R., et al., *Detection of local ATP release from activated platelets using cell surface-attached firefly luciferase.* Am J Physiol, 1999. **276**(1): p. C267-78.
19. Pellegatti, P., et al., *A novel recombinant plasma membrane-targeted luciferase reveals a new pathway for ATP secretion.* Mol Biol Cell, 2005. **16**(8): p. 3659-65.
20. De Marchi, E., et al., *Detection of Extracellular ATP in the Tumour Microenvironment, Using the pmeLUC Biosensor.* Methods Mol Biol, 2020. **2041**: p. 183-195.
21. Lustig, K.D., et al., *Expression cloning of an ATP receptor from mouse neuroblastoma cells.* Proc Natl Acad Sci U S A, 1993. **90**(11): p. 5113-7.
22. Webb, T.E., et al., *Cloning and functional expression of a brain G-protein-coupled ATP receptor.* FEBS Lett, 1993. **324**(2): p. 219-25.
23. Brake, A.J., M.J. Wagenbach, and D. Julius, *New structural motif for ligand-gated ion channels defined by an ionotropic ATP receptor.* Nature, 1994. **371**(6497): p. 519-23.
24. Burnstock, G. and C. Kennedy, *Is there a basis for distinguishing two types of P2-purinoceptor?* Gen Pharmacol, 1985. **16**(5): p. 433-40.
25. Jacobson, K.A. and C.E. Muller, *Medicinal chemistry of adenosine, P2Y and P2X receptors.* Neuropharmacology, 2016. **104**: p. 31-49.
26. North, R.A. and A. Surprenant, *Pharmacology of cloned P2X receptors.* Annu Rev Pharmacol Toxicol, 2000. **40**: p. 563-80.
27. Kawate, T., et al., *Crystal structure of the ATP-gated P2X(4) ion channel in the closed state.* Nature, 2009. **460**(7255): p. 592-8.
28. Compan, V., et al., *P2X2 and P2X5 subunits define a new heteromeric receptor with P2X7-like properties.* J Neurosci, 2012. **32**(12): p. 4284-96.
29. Ferrari, D., et al., *The antibiotic polymyxin B modulates P2X7 receptor function.* J Immunol, 2004. **173**(7): p. 4652-60.
30. Di Virgilio, F. and M. Vuerich, *Purinergic signaling in the immune system.* Auton Neurosci, 2015. **191**: p. 117-23.
31. Di Virgilio, F., et al., *Extracellular ATP and P2 purinergic signalling in the tumour microenvironment.* Nat Rev Cancer, 2018.
32. Burnstock, G. and A. Verkhratsky, *Long-term (trophic) purinergic signalling: purinoceptors control cell proliferation, differentiation and death.* Cell Death Dis, 2010. **1**: p. e9.

33. Burnstock, G. and G.E. Knight, *Cellular distribution and functions of P2 receptor subtypes in different systems.* Int Rev Cytol, 2004. **240**: p. 31-304.
34. Buell, G.N., et al., *Gene structure and chromosomal localization of the human P2X7 receptor.* Receptors Channels, 1998. **5**(6): p. 347-54.
35. Surprenant, A., et al., *The cytolytic P2Z receptor for extracellular ATP identified as a P2X receptor (P2X7).* Science, 1996. **272**(5262): p. 735-8.
36. Karasawa, A. and T. Kawate, *Structural basis for subtype-specific inhibition of the P2X7 receptor.* Elife, 2016. **5**.
37. McCarthy, A.E., C. Yoshioka, and S.E. Mansoor, *Full-Length P2X7 Structures Reveal How Palmitoylation Prevents Channel Desensitization.* Cell, 2019. **179**(3): p. 659-670 e13.
38. Hattori, M. and E. Gouaux, *Molecular mechanism of ATP binding and ion channel activation in P2X receptors.* Nature, 2012. **485**(7397): p. 207-12.
39. Di Virgilio, F., et al., *Fura-2 secretion and sequestration in macrophages. A blocker of organic anion transport reveals that these processes occur via a membrane transport system for organic anions.* J Immunol, 1988. **140**(3): p. 915-20.
40. Adinolfi, E., et al., *Trophic activity of a naturally occurring truncated isoform of the P2X7 receptor.* FASEB J, 2010. **24**(9): p. 3393-404.
41. Adinolfi, E., et al., *Basal activation of the P2X7 ATP receptor elevates mitochondrial calcium and potential, increases cellular ATP levels, and promotes serum-independent growth.* Mol Biol Cell, 2005. **16**(7): p. 3260-72.
42. Cheewatrakoolpong, B., et al., *Identification and characterization of splice variants of the human P2X7 ATP channel.* Biochem Biophys Res Commun, 2005. **332**(1): p. 17-27.
43. Sluyter, R. and L. Stokes, *Significance of P2X7 receptor variants to human health and disease.* Recent Pat DNA Gene Seq, 2011. **5**(1): p. 41-54.
44. Feng, Y.H., et al., *A truncated P2X7 receptor variant (P2X7-j) endogenously expressed in cervical cancer cells antagonizes the full-length P2X7 receptor through hetero-oligomerization.* J Biol Chem, 2006. **281**(25): p. 17228-37.
45. Giuliani, A.L., et al., *Trophic activity of human P2X7 receptor isoforms A and B in osteosarcoma.* PLoS One, 2014. **9**(9): p. e107224.
46. Ulrich, H., et al., *Kinin and Purine Signaling Contributes to Neuroblastoma Metastasis.* Front Pharmacol, 2018. **9**: p. 500.
47. Carluccio, M., et al., *Involvement of P2X7 Receptors in the Osteogenic Differentiation of Mesenchymal Stromal/Stem Cells Derived from Human Subcutaneous Adipose Tissue.* Stem Cell Rev Rep, 2019. **15**(4): p. 574-589.
48. Jacobson, K.A., M.F. Jarvis, and M. Williams, *Purine and pyrimidine (P2) receptors as drug targets.* J Med Chem, 2002. **45**(19): p. 4057-93.

49. De Marchi, E., et al., *P2X7 Receptor as a Therapeutic Target.* Adv Protein Chem Struct Biol, 2016. **104**: p. 39-79.
50. Evans, R.J., et al., *Pharmacological characterization of heterologously expressed ATP-gated cation channels (P2x purinoceptors).* Mol Pharmacol, 1995. **48**(2): p. 178-83.
51. Nelson, D.W., et al., *Structure-activity relationship studies on a series of novel, substituted 1-benzyl-5-phenyltetrazole P2X7 antagonists.* J Med Chem, 2006. **49**(12): p. 3659-66.
52. Honore, P., et al., *A-740003 [N-(1-{[(cyanoimino)(5-quinolinylamino) methyl]amino}-2,2-dimethylpropyl)-2-(3,4-dimethoxyphenyl)acetamide], a novel and selective P2X7 receptor antagonist, dose-dependently reduces neuropathic pain in the rat.* J Pharmacol Exp Ther, 2006. **319**(3): p. 1376-85.
53. King, B.F., *Novel P2X7 receptor antagonists ease the pain.* Br J Pharmacol, 2007. **151**(5): p. 565-7.
54. Adinolfi, E., et al., *Expression of P2X7 receptor increases in vivo tumour growth.* Cancer Res, 2012. **72**(12): p. 2957-69.
55. Amoroso, F., et al., *The P2X7 receptor is a key modulator of the PI3K/GSK3beta/VEGF signaling network: evidence in experimental neuroblastoma.* Oncogene, 2015. **34**(41): p. 5240-51.
56. Di Virgilio, F., et al., *The P2X7 Receptor in Infection and Inflammation.* Immunity, 2017. **47**(1): p. 15-31.
57. Burnstock, G. and F. Di Virgilio, *Purinergic signalling and cancer.* Purinergic Signal, 2013. **9**(4): p. 491-540.
58. Dinarello, C.A., *Interleukin-1beta and the autoinflammatory diseases.* N Engl J Med, 2009. **360**(23): p. 2467-70.
59. Dinarello, C.A., *The IL-1 family and inflammatory diseases.* Clin Exp Rheumatol, 2002. **20**(5 Suppl 27): p. S1-13.
60. Adinolfi, E., et al., *The P2X7 receptor: A main player in inflammation.* Biochem Pharmacol, 2018. **151**: p. 234-244.
61. Ferrari, D., et al., *Extracellular ATP triggers IL-1 beta release by activating the purinergic P2Z receptor of human macrophages.* J Immunol, 1997. **159**(3): p. 1451-8.
62. Alves, L.A., et al., *Physiological roles and potential therapeutic applications of the P2X7 receptor in inflammation and pain.* Molecules, 2013. **18**(9): p. 10953-72.
63. Caporali, F., et al., *Human rheumatoid synoviocytes express functional P2X7 receptors.* J Mol Med (Berl), 2008. **86**(8): p. 937-49.
64. Di Virgilio, F. and A.L. Giuliani, *Purinergic signalling in autoimmunity: A role for the P2X7 in systemic lupus erythematosus?* Biomed J, 2016. **39**(5): p. 326-338.

65. Turner, C.M., et al., *Increased expression of the pro-apoptotic ATP-sensitive P2X7 receptor in experimental and human glomerulonephritis.* Nephrol Dial Transplant, 2007. **22**(2): p. 386-95.
66. Slater, M., et al., *Differentiation between cancerous and normal hyperplastic lobules in breast lesions.* Breast Cancer Res Treat, 2004. **83**(1): p. 1-10.
67. Slater, M., et al., *Early prostate cancer detected using expression of non-functional cytolytic P2X7 receptors.* Histopathology, 2004. **44**(3): p. 206-15.
68. Li, X., et al., *The P2X7 receptor: a novel biomarker of uterine epithelial cancers.* Cancer Epidemiol Biomarkers Prev, 2006. **15**(10): p. 1906-13.
69. White, N., P.E. Butler, and G. Burnstock, *Human melanomas express functional P2 X(7) receptors.* Cell Tissue Res, 2005. **321**(3): p. 411-8.
70. Raffaghello, L., et al., *The P2X7 receptor sustains the growth of human neuroblastoma cells through a substance P-dependent mechanism.* Cancer Res, 2006. **66**(2): p. 907-14.
71. Solini, A., et al., *Increased P2X7 receptor expression and function in thyroid papillary cancer: a new potential marker of the disease?* Endocrinology, 2008. **149**(1): p. 389-96.
72. Adinolfi, E., et al., *P2X7 receptor expression in evolutive and indolent forms of chronic B lymphocytic leukemia.* Blood, 2002. **99**(2): p. 706-8.
73. Rossi, L., et al., *The sixth sense: hematopoietic stem cells detect danger through purinergic signaling.* Blood, 2012. **120**(12): p. 2365-75.
74. Zhang, X.J., et al., *Expression of P2X7 in human hematopoietic cell lines and leukemia patients.* Leuk Res, 2004. **28**(12): p. 1313-22.
75. Jelassi, B., et al., *Anthraquinone emodin inhibits human cancer cell invasiveness by antagonizing P2X7 receptors.* Carcinogenesis, 2013. **34**(7): p. 1487-96.
76. Jelassi, B., et al., *P2X(7) receptor activation enhances SK3 channels- and cystein cathepsin-dependent cancer cells invasiveness.* Oncogene, 2011. **30**(18): p. 2108-22.
77. Adinolfi, E., et al., *Emerging roles of P2X receptors in cancer.* Curr Med Chem, 2015. **22**(7): p. 878-90.
78. Hofman, P., et al., *Genetic and pharmacological inactivation of the purinergic P2RX7 receptor dampens inflammation but increases tumour incidence in a mouse model of colitis-associated cancer.* Cancer Res, 2015. **75**(5): p. 835-45.
79. Bianchi, G., et al., *ATP/P2X7 axis modulates myeloid-derived suppressor cell functions in neuroblastoma microenvironment.* Cell Death Dis, 2014. **5**: p. e1135.
80. Lecciso, M., et al., *ATP Release from Chemotherapy-Treated Dying Leukemia Cells Elicits an Immune Suppressive Effect by Increasing Regulatory T Cells and Tolerogenic Dendritic Cells.* Front Immunol, 2017. **8**: p. 1918.

81. De Marchi, E., et al., *The P2X7 receptor modulates immune cells infiltration, ectonucleotidases expression and extracellular ATP levels in the tumour microenvironment.* Oncogene, 2019. **38**(19): p. 3636-3650.
82. Falk, S., et al., *P2X7 receptor-mediated analgesia in cancer-induced bone pain.* Neuroscience, 2015. **291**: p. 93-105.
83. Amoroso, F., et al., *The P2X7 receptor is a key modulator of aerobic glycolysis.* Cell Death Dis, 2012. **3**: p. e370.
84. Xia, J., et al., *P2X7 receptor stimulates breast cancer cell invasion and migration via the AKT pathway.* Oncol Rep, 2015. **34**(1): p. 103-10.
85. Takai, E., et al., *Autocrine regulation of TGF-beta1-induced cell migration by exocytosis of ATP and activation of P2 receptors in human lung cancer cells.* J Cell Sci, 2012. **125**(Pt 21): p. 5051-60.
86. Hattori, F., et al., *Feasibility study of B16 melanoma therapy using oxidized ATP to target purinergic receptor P2X7.* Eur J Pharmacol, 2012. **695**(1-3): p. 20-6.
87. Adinolfi, E., et al., *Expression of the P2X7 receptor increases the Ca2+ content of the endoplasmic reticulum, activates NFATc1, and protects from apoptosis.* J Biol Chem, 2009. **284**(15): p. 10120-8.
88. Adinolfi, E., F. Amoroso, and A.L. Giuliani, *P2X7 Receptor Function in Bone-Related Cancer.* J Osteoporos, 2012. **2012**: p. 637863.
89. Solini, A., et al., *Genetic interaction of P2X7 receptor and VEGFR-2 polymorphisms identifies a favorable prognostic profile in prostate cancer patients.* Oncotarget, 2015. **6**(30): p. 28743-54.
90. Chong, J.H., et al., *Abnormal expression of P2X family receptors in Chinese pediatric acute leukemias.* Biochem Biophys Res Commun, 2010. **391**(1): p. 498-504.
91. Gu, L.Q., et al., *Association of XIAP and P2X7 receptor expression with lymph node metastasis in papillary thyroid carcinoma.* Endocrine, 2010. **38**(2): p. 276-82.
92. Gehring, M.P., et al., *P2X7 receptor activation leads to increased cell death in a radiosensitive human glioma cell line.* Purinergic Signal, 2012. **8**(4): p. 729-39.
93. Gehring, M.P., et al., *P2X7 receptor as predictor gene for glioma radiosensitivity and median survival.* Int J Biochem Cell Biol, 2015. **68**: p. 92-100.
94. Akers, J.C., et al., *Biogenesis of extracellular vesicles (EV): exosomes, microvesicles, retrovirus-like vesicles, and apoptotic bodies.* J Neurooncol, 2013. **113**(1): p. 1-11.
95. Raposo, G. and W. Stoorvogel, *Extracellular vesicles: exosomes, microvesicles, and friends.* J Cell Biol, 2013. **200**(4): p. 373-83.
96. van der Pol, E., et al., *Classification, functions, and clinical relevance of extracellular vesicles.* Pharmacol Rev, 2012. **64**(3): p. 676-705.

97. Webber, J., et al., *Cancer exosomes trigger fibroblast to myofibroblast differentiation.* Cancer Res, 2010. **70**(23): p. 9621-30.

98. Valadi, H., et al., *Exosome-mediated transfer of mRNAs and microRNAs is a novel mechanism of genetic exchange between cells.* Nat Cell Biol, 2007. **9**(6): p. 654-9.

99. Tauro, B.J., et al., *Oncogenic H-ras reprograms Madin-Darby canine kidney (MDCK) cell-derived exosomal proteins following epithelial-mesenchymal transition.* Mol Cell Proteomics, 2013. **12**(8): p. 2148-59.

100. Chen, W., et al., *Efficient induction of antitumour T cell immunity by exosomes derived from heat-shocked lymphoma cells.* Eur J Immunol, 2006. **36**(6): p. 1598-607.

101. Hoshino, A., et al., *Tumour exosome integrins determine organotropic metastasis.* Nature, 2015. **527**(7578): p. 329-35.

102. MacKenzie, A., et al., *Rapid secretion of interleukin-1beta by microvesicle shedding.* Immunity, 2001. **15**(5): p. 825-35.

103. Bianco, F., et al., *Astrocyte-derived ATP induces vesicle shedding and IL-1 beta release from microglia.* J Immunol, 2005. **174**(11): p. 7268-77.

104. Pizzirani, C., et al., *Stimulation of P2 receptors causes release of IL-1beta-loaded microvesicles from human dendritic cells.* Blood, 2007. **109**(9): p. 3856-64.

105. Gulinelli, S., et al., *IL-18 associates to microvesicles shed from human macrophages by a LPS/TLR-4 independent mechanism in response to P2X receptor stimulation.* Eur J Immunol, 2012. **42**(12): p. 3334-45.

106. Barbera-Cremades, M., et al., *P2X7 Receptor Induces Tumour Necrosis Factor-alpha Converting Enzyme Activation and Release to Boost TNF-alpha Production.* Front Immunol, 2017. **8**: p. 862.

107. Baroni, M., et al., *Stimulation of P2 (P2X7) receptors in human dendritic cells induces the release of tissue factor-bearing microparticles.* FASEB J, 2007. **21**(8): p. 1926-33.

108. Sobrevia, L. and B.B. Fredholm, *Adenosine - from molecular mechanisms to pathophysiology.* Mol Aspects Med, 2017. **55**: p. 1-3.

109. Chen, K. and N. Rajewsky, *The evolution of gene regulation by transcription factors and microRNAs.* Nat Rev Genet, 2007. **8**(2): p. 93-103.

110. Bartel, D.P., *MicroRNAs: target recognition and regulatory functions.* Cell, 2009. **136**(2): p. 215-33.

111. Brinton, L.T., et al., *Formation and role of exosomes in cancer.* Cell Mol Life Sci, 2015. **72**(4): p. 659-71.

112. Pfeffer, S.R., et al., *Detection of Exosomal miRNAs in the Plasma of Melanoma Patients.* J Clin Med, 2015. **4**(12): p. 2012-27.

113. Ye, S.B., et al., *Tumour-derived exosomes promote tumour progression and T-cell dysfunction through the regulation of enriched exosomal microRNAs in human nasopharyngeal carcinoma.* Oncotarget, 2014. **5**(14): p. 5439-52.
114. Lee, J.C., et al., *Papillary thyroid cancer-derived exosomes contain miRNA-146b and miRNA-222.* J Surg Res, 2015. **196**(1): p. 39-48.
115. Haug, B.H., et al., *Exosome-like Extracellular Vesicles from MYCN-amplified Neuroblastoma Cells Contain Oncogenic miRNAs.* Anticancer Res, 2015. **35**(5): p. 2521-30.
116. Garajova, I., et al., *Non-Coding RNAs as Predictive Biomarkers to Current Treatment in Metastatic Colorectal Cancer.* Int J Mol Sci, 2017. **18**(7).
117. Di Stefano, C., et al., *The roles of microRNAs in the pathogenesis and drug resistance of chronic myelogenous leukemia (Review).* Oncol Rep, 2016. **35**(2): p. 614-24.
118. Fong, M.Y., et al., *Breast-cancer-secreted miR-122 reprograms glucose metabolism in premetastatic niche to promote metastasis.* Nat Cell Biol, 2015. **17**(2): p. 183-94.
119. Mocharla, P., et al., *AngiomiR-126 expression and secretion from circulating CD34(+) and CD14(+) PBMCs: role for proangiogenic effects and alterations in type 2 diabetics.* Blood, 2013. **121**(1): p. 226-36.
120. Zhang, L., et al., *Microenvironment-induced PTEN loss by exosomal microRNA primes brain metastasis outgrowth.* Nature, 2015. **527**(7576): p. 100-104.
121. Ferrara, F. and C.A. Schiffer, *Acute myeloid leukaemia in adults.* Lancet, 2013. **381**(9865): p. 484-95.
122. Deschler, B. and M. Lubbert, *Acute myeloid leukemia: epidemiology and etiology.* Cancer, 2006. **107**(9): p. 2099-107.
123. Becha, M. and N. Braham Jmili, *[Myelodysplastic syndromes: pathophysiology, clinical and biological features].* Ann Biol Clin (Paris), 2015. **73**(6): p. 643-56.
124. De Kouchkovsky, I. and M. Abdul-Hay, *'Acute myeloid leukemia: a comprehensive review and 2016 update'.* Blood Cancer J, 2016. **6**(7): p. e441.
125. Arber, D.A., et al., *The 2016 revision to the World Health Organization classification of myeloid neoplasms and acute leukemia.* Blood, 2016. **127**(20): p. 2391-405.
126. Di Marco, A., G. Cassinelli, and F. Arcamone, *The discovery of daunorubicin.* Cancer Treat Rep, 1981. **65 Suppl 4**: p. 3-8.
127. Dombret, H. and C. Gardin, *An update of current treatments for adult acute myeloid leukemia.* Blood, 2016. **127**(1): p. 53-61.
128. Schiller, G.J., *High-Intensity Induction in the Elderly.* Acta Haematol, 2016. **135**(1): p. 53-4.
129. Tan, C., et al., *Daunomycin, an antitumour antibiotic, in the treatment of neoplastic disease. Clinical evaluation with special reference to childhood leukemia.* Cancer, 1967. **20**(3): p. 333-53.

130. Galaris, D., A. Georgellis, and J. Rydstrom, *Toxic effects of daunorubicin on isolated and cultured heart cells from neonatal rats.* Biochem Pharmacol, 1985. **34**(7): p. 989-95.
131. Stein, E.M. and M.S. Tallman, *Novel and emerging drugs for acute myeloid leukemia.* Curr Cancer Drug Targets, 2012. **12**(5): p. 522-30.
132. Moan, J., A.C. Porojnicu, and A. Dahlback, *Ultraviolet radiation and malignant melanoma.* Adv Exp Med Biol, 2008. **624**: p. 104-16.
133. Franken, M.G., et al., *A systematic literature review and network meta-analysis of effectiveness and safety outcomes in advanced melanoma.* Eur J Cancer, 2019. **123**: p. 58-71.
134. Livingstone, A., et al., *Preferences for Immunotherapy in Melanoma: A Systematic Review.* Ann Surg Oncol, 2019.
135. Iannone, R., et al., *Adenosine limits the therapeutic effectiveness of anti-CTLA4 mAb in a mouse melanoma model.* Am J Cancer Res, 2014. **4**(2): p. 172-81.
136. Slater, M., et al., *Increased expression of apoptotic markers in melanoma.* Melanoma Res, 2003. **13**(2): p. 137-45.
137. Salvestrini, V., et al., *Extracellular ATP induces apoptosis through P2X7 activation in acute myeloid leukemia cells but not in normal hematopoietic stem cells.* Oncotarget, 2017. **8**(4): p. 5895-5908.
138. Lemaire, I., et al., *Involvement of the purinergic P2X7 receptor in the formation of multinucleated giant cells.* J Immunol, 2006. **177**(10): p. 7257-65.
139. Munerati, M., et al., *Macrophages loaded with doxorubicin by ATP-mediated permeabilization: potential carriers for antitumour therapy.* Biochim Biophys Acta, 1994. **1224**(2): p. 269-76.
140. Di Virgilio, F. and E. Adinolfi, *Extracellular purines, purinergic receptors and tumour growth.* Oncogene, 2017. **36**(3): p. 293-303.